Erythrocytosis-inducing PHD2 mutations implicate biological role for N-terminal prolyl-hydroxylation in HIF1α oxygen-dependent degradation domain

Cassandra C. Taber[1], Wenguang He[1,2], Geneviève M. C. Gasmi-Seabrook[3], Mia Hubert[1], Fraser G. Ferens[1], Mitsuhiko Ikura[3,4], Jeffrey E. Lee[1], Michael Ohh[1,2,*]

[1] Department of Laboratory Medicine and Pathobiology, Temerty Faculty of Medicine, University of Toronto, 1 King's College Circle, Toronto, ON M5S 1A8, Canada

[2] Department of Biochemistry, Temerty Faculty of Medicine, University of Toronto, 661 University Avenue, Toronto, ON M5G 1M1, Canada

[3] Princess Margaret Cancer Centre, University Health Network, Toronto, ON M5G 2C4, Canada

[4] Department of Medical Biophysics, Temerty Faculty of Medicine, University of Toronto, 610 University Avenue, Toronto, ON M5G 1L7, Canada

[*] Address correspondence to: Prof. Michael Ohh; Tel. +1 (416) 946-7922; E-mail: michael.ohh@utoronto.ca

ABSTRACT

Mutations in *EGLN1*, the gene encoding for hypoxia-inducible factor (HIF) prolyl-4-hydroxylase 2 (PHD2), cause erythrocytosis and in rare cases the development of neuroendocrine tumors. In the presence of oxygen, PHD2 hydroxylates one or both conserved prolines in the oxygen-dependent degradation domain (ODD) of HIFα subunits, sufficiently marking HIFα for binding and ubiquitylation via the von Hippel-Lindau (VHL) tumor suppressor protein-containing E3 ubiquitin ligase and subsequent degradation by the 26S proteasome. However, prolyl-hydroxylation in the C-terminal ODD appears to be the predominant and sufficient event in triggering the oxygen-dependent destruction of HIFα, rendering the biological significance of N-terminal ODD proline unclear. Here, we examined 7 disease-associated *EGLN1* mutations scattered across the catalytic core and show definitively that all PHD2 mutants have a structural and/or catalytic activity defect as measured by time-resolved nuclear magnetic resonance. Notably, we identified one of the PHD2 mutants, P317R, to retain comparably wild-type capacity to hydroxylate the predominant proline in the C-terminal ODD but had uniquely compromised ability to hydroxylate the N-terminal ODD proline. These findings support the notion that deregulation of HIF ultimately underlies PHD2-driven erythrocytosis and challenge the currently held uncertainty that the N-terminal ODD prolyl-hydroxylation event is dispensable in normal hypoxic signaling pathway.

INTRODUCTION

About half of blood volume is made up of erythrocytes (red blood cells) whose role is to deliver oxygen from the lungs to the tissues in the body[1]. Low concentrations of red blood cells result in insufficient oxygen delivery to tissues while high concentrations can induce a propensity towards thrombotic events rendering red blood cell mass regulation crucial. Erythropoietin (EPO) is a hormone produced primarily in the kidneys that stimulates erythropoiesis[2,3]. Through binding to EPO receptors on erythroid progenitors, EPO can activate a signaling cascade that induces differentiation into erythrocytes[4]. EPO production is regulated in response to physiological oxygen concentrations through hypoxia response elements (HRE). HREs are enhancers that transcription factors called hypoxia-inducible factors (HIFs) bind to and subsequently upregulate the expression of numerous hypoxic response genes including *EPO*[5]. Disrupted EPO regulation can be pathogenic and lead to an autonomous overproduction of erythrocytes causing erythrocytosis[6]. Due to EPO's inherent link to the oxygen response, mutations in the metazoan oxygen-sensing pathway have frequently been found to underlie erythrocytosis.

The oxygen-sensing pathway has been conserved in all animals and is essential for the maintenance of cellular activities in low oxygen settings[7]. Under hypoxia, oxygen-labile HIF1-3α subunits complex with its constitutively expressed HIFβ subunits to translocate to the nucleus as active heterodimeric transcription factors[8]. Following translocation, HIF binds to HREs across the genome to trigger the transactivation of numerous genes such as *GLUT1*, *EPO* and *VEGF* to promote anaerobic metabolism, erythropoiesis and angiogenesis, respectively, to induce adaptation to low oxygen availability[9]. In normal oxygen conditions, HIF prolyl hydroxylases (PHDs) hydroxylate HIFα subunit at one or both of the two conserved proline sites located in the oxygen-dependent degradation domain (ODD), which initiates its ubiquitylation via the von Hippel-Lindau tumor suppressor protein (pVHL)-containing E3 ubiquitin ligase (Elongin BC/Cullin 2-Rbx1/pVHL) and subsequent destruction via the 26S proteasome. Notably, only one proline is required to be hydroxylated to trigger its rapid destruction and whether HIFα is singly or doubly hydroxylated does not appear to change the rate of its ubiquitylation or proteasome-mediated destruction[10]. Moreover, the C-terminally located proline within ODD or CODD (e.g., P564 on HIF1α) has been shown to be the predominant residue that becomes hydroxylated prior to the modification of proline in the N-terminal ODD or NODD (e.g., P402 on HIF1α)[10-12]. The reason for this preferential prolyl-hydroxylation is incompletely understood, and the biological significance or the mechanistic purpose of the N-terminal proline remains unclear.

Clinically observed mutations have been identified in the major components of the oxygen-sensing pathway including *VHL (*pVHL*)*[13,14]*, EPAS1* (HIF2α)[15-17]*, EGLN1* (PHD2)[18,19], and *EGLN2* (PHD1)[20]. These have been associated with the development of diseases with overlapping phenotypes with erythrocytosis being the most common. Collectively, these diseases are referred to as pseudohypoxic diseases as they involve an inappropriate hypoxic response. Erythrocytosis caused by mutations in *EGLN1* is the most recently discovered pseudohypoxic disease. Since its first reported case in 2006[21], 152 cases with 96 distinct mutations have been reported (**Supplementary Data**). *EGLN1* mutation-driven erythrocytosis is referred to as erythrocytosis, familial, 3 (ECYT3) by the Online Mendelian Inheritance in Man (OMIM). However, three individuals with distinct *EGLN1* mutations (W51X, A228S and H374R) developed recurrent pheochromocytoma and paraganglioma (PPGL)[20,22,23], which are neuroendocrine tumors that develop from chromaffin cells either within (pheochromocytoma) or outside (paraganglioma) the adrenal gland[24].

Of three isozymes of PHD, PHD2 is thought to be the most critical with high expression seen in a variety of cell types [25] and the only PHD able to effectively target both prolines in HIF1α and 2α ODDs[11,26,27]. PHD2 belongs to the 2-oxoglutarate-dependent-dioxygenase superfamily[28] in which enzymes contain a double-stranded β-helix fold with a highly conserved HXE/D...H motif that coordinates Fe^{2+} at its catalytic site[29]. In PHD2, the iron coordinating residues are His313, Asp315 and His374[30]. Erythrocytosis-causing mutations at (H374R) and near these conserved catalytic residues have been shown to be defective at regulating HIFα in a cellular context[18,21,23], which appears to be a common mechanism observed in the other pseudohypoxic diseases. For example, numerous studies have revealed that pVHL mutants have varied abilities to recognize and regulate HIFα leading to the development of PPGL, erythrocytosis and other cancers such as clear-cell renal cell carcinoma and hemangioblastoma[31-33]. Recently, we showed that phenotypic severity of Pacak-Zhuang syndrome, caused by *EPAS1* mutations, is correlated to the ability of HIF2α mutants to escape degradation mediated by pVHL and PHD2[15,34].

Together, these observations suggest that disproportionately high levels of HIFα are responsible for pseudohypoxic disease phenotypes such as erythrocytosis and PPGL. In keeping with this notion, disease-causing mutants of PHD2 are likely defective in catalyzing HIFα hydroxylation to some extent, resulting in less HIFα degradation and correspondingly increased hypoxia response signaling. However, the precise mechanism(s) underlying such defect in PHD2 function is unclear. Recently, we devised a time-resolved nuclear magnetic resonance (NMR)

assay to directly measure the rate of hydroxylation on the two conserved proline residues simultaneously in HIF1α ODD[12]. Here, we examined 7 disease-associated PHD2 mutants via biophysical analyses and show that all PHD2 mutants have structural and/or catalytic activity defects. While all mutants had the anticipated defect in binding and hydroxylating the predominant CODD proline, we identified PHD2 P317R mutant that retained comparably wild-type level of hydroxylating CODD proline (i.e., HIF1α P564) but failed to hydroxylate NODD proline (i.e., HIF1α P402) as measured by NMR. Unexpectedly, PHD2 P317R was capable of binding to both NODD and CODD peptides with similar affinity. These results provide a biophysical mechanism that, at least in part, underlies PHD2-driven erythrocytosis, and serendipitously reveal direct biochemical evidence to suggest that NODD prolyl-hydroxylation is necessary for normal physiological response to hypoxia.

RESULTS

Mutations across the PHD2 enzyme induce erythrocytosis

We compiled and analyzed all reported cases of PHD2-driven erythrocytosis as of January 2025. 96 distinct variants have been reported, including two missense variants commonly found in Tibetan populations that are hypothesized to be adaptations to high altitude conditions (D4E and C127S)[35,36]. Consistent with erythrocytosis in the general population, most patients with PHD2-driven erythrocytosis were male (~70%). About half of the case reports provided information on family history of PHD2-driven erythrocytosis, of which ~75% were reported to be familial while ~25% were *de novo* mutations; a similar rate of *de novo* mutations is observed with VHL disease. PHD2-driven erythrocytosis is typically classified as secondary erythrocytosis, which is defined as being caused by an EPO-inducing mechanism downstream of the primary defect, ultimately resulting in normal to high EPO levels that drive erythropoiesis. This classification is aligned with the suspected mechanism of PHD2-driven disease in which mutated PHD2 dysregulates HIF leading to increased EPO production. Curiously however, EPO was reported to be largely normal in patients with PHD2-driven erythrocytosis with few exceptions (**Supplementary Data**), which is consistent with the loss of PHD2 in mice leading to EPO hypersensitivity in erythroid progenitors, enabling a 'normal' amount of EPO to generate a pathogenic response[37].

All cases of PHD2-driven erythrocytosis were reported as germline heterozygous mutations of PHD2, suggesting haploinsufficiency of PHD2 is enough to induce erythrocytosis. This is consistent with previous reports that HIFα regulation is dose dependent on PHD2 knockdown via

siRNA[25]. As stated previously, in three exceptional cases, individuals with PHD2 mutations developed PPGL (W51X, A228S and H374R). Biopsies of each tumor revealed a loss of heterozygosity for PHD2, implying a complete loss of wild-type PHD2 in chromaffin cells is necessary to induce tumorigenesis.

The majority of the reported mutations were missense (~74%) (**Figure 1A**). Interestingly, mutations that should theoretically severely disrupt PHD2 structure (nonsense, frameshift and deletions) caused the same phenotype (erythrocytosis) as less disruptive missense mutations, suggesting an unclear or lack of correlation between mutation type and phenotypic severity. Thus, a potential phenotypic mechanism of PHD2-driven disease can be hypothesized where erythrocytosis will develop upon deleterious mutation in one PHD2 allele while PPGL will be induced upon a loss of heterozygosity in chromaffin cells.

Mutations are distributed across all exons of PHD2 with some clustering across the catalytic core (**Figure 1B**). When mapped onto the three-dimensional crystal structure of the PHD2 catalytic core, which we and others have previously solved[34,38,39], these mutations do not seem to display a specific pattern (**Figure 1C**). Accordingly, representative PHD2 mutants were selected to analyze the mechanism of disease caused by PHD2 mutations. Some mutants were chosen based on their frequency in the clinical data and their presence in potential mutational hot spots. Various mutations were noted at W334 and R371 sites, while F366L was identified in multiple individuals. 9 cases of PHD2-driven disease were reported to be caused from mutations located between residues 200 to 210 while 13 cases were reported between residues 369-379. Thus, G206C and R371H were chosen to represent these potential hot spots. To examine a potential genotype-phenotype relationship, two of the mutants, A228S and H374R, responsible for neuroendocrine tumor development were also selected. Finally, mutations located close or on catalytic core residues (P317R, R371H, and H374R) were chosen to test for suspected defects. Ultimately, we selected 7 PHD2 mutants with distinct residue changes in the catalytic core of PHD2 for study.

Some PHD2 mutants are less stable and defective in regulating HRE-driven transcription

We asked whether the enzymatic activity of PHD2 mutants can be inferred from downstream HIF activity using a dual luciferase reporter assay under control of HRE. Notably, we first generated CRISPR/Cas9-mediated PHD2 knockout (-/-) HEK293A cells to minimize the impact of endogenous PHD2 on the prolyl-hydroxylation of HIFα. As expected, wild-type (WT) ectopic PHD2 markedly reduced the HRE-luciferase activity driven by ectopic HIF1α compared to cells without ectopic

PHD2 expression (**Figure 2A**). Two disease-associated PHD2 mutants, P317R and H374R, displayed significantly reduced ability to knockdown luciferase activity (~2-fold and ~2.5-fold, respectively) compared to PHD2 WT. Notably, the other mutants showed comparable activity to PHD2 WT in down-regulating HRE-driven luciferase signal under these *in cellulo* experimental conditions (**Figure 2A**).

We next performed cycloheximide (CHX) chase assay to determine the protein stability of PHD2 mutants. We observed that mutants G206C, W334R, F366L, R371H, and H374R showed noticeable instability by 24 hours (**Figure 2B** and **C**). These results suggest that while most PHD mutants showed diminished protein stability in comparison to PHD2 WT, the stability of PHD2 mutants cannot alone explain the impact of these disease-associated mutations on HIF1α-driven HRE-luciferase activity in cells.

PHD2 mutants are thermally unstable and some are prone to aggregation

We asked if the disease-causing mutations compromised other biophysical characteristics of PHD2. We purified catalytic cores of PHD2 harboring the selected mutations for the subsequent biophysical studies. Size exclusion chromatography (SEC) was performed as a polishing step and chromatograms were acquired with monomeric PHD2 eluting from the column around 16.5 mL (**Figure 3A**). Mutants were eluted from the column at different volumes ranging from 16.2 mL (G206C) to 16.7 mL (P317R), while WT PHD2 was eluted consistently at 16.5 mL. These results suggest that mutations may affect the hydrodynamic size of PHD2, hinting to mutation-induced structural alteration. Moreover, PHD2 G206C, W334R and H374R aggregated severely in SEC and throughout the purification process and could not be purified.

We next subjected the remaining four mutants (A228S, P317R, F366L, and R371H) in comparison to WT PHD2 to circular dichroism (CD) to determine structural abnormalities. The CD spectra of the mutant PHD2s did not display appreciable differences from WT PHD2 (**Figure 3B**), indicating that these PHD2 mutants' overall structure is mostly unaffected.

To further probe the stability of PHD2 mutants, molar ellipticity was measured at 220 nm from 25 to 95 °C to determine melting temperature (T_m). Alpha helices produce a strong minimum at 220 nm so this wavelength was selected to measure thermal protein unfolding[40]. Melting curves were created by setting the peak value of each spectrum at 25 °C to 1.0. The data were then fitted with a sigmoidal curve to produce melting curves and calculate T_m's (**Figure 3C** and **Table 1**). WT PHD2's T_m, estimated as the temperature at which half of the proteins are unfolded, was

determined to be 52.3°C. All four mutants had lower T_m's than WT, suggesting a degree of thermal instability. Although it is reasonable to assume that instability would result in less PHD2, it is unclear if the unstable enzyme is active prior to degradation and whether the remaining portion of mutant PHD2s would be sufficient to bind and hydroxylate HIFα.

PHD2 mutants have weaker binding to HIFα than WT PHD2

Assuming intact catalytic function, the strength of PHD2 binding affinity to HIFα should translate to the extent of prolyl-hydroxylation of HIFα via PHD2. We performed microscale thermophoresis (MST), which utilizes the motion of molecules in a temperature gradient to determine dissociation constants (K_d), to measure the binding deficiencies, if any, between PHD2 mutants and HIFα. In addition to being highly sensitive, MST is also advantageous for measuring protein-ligand binding in an untethered setting. We showed previously that this technique was effective at distinguishing between disease classes of HIF2α mutants in Pacak-Zhuang syndrome by measuring their binding affinities to WT PHD2[34]. We performed a similar protocol with PHD2 mutants to identify potential binding defects with HIF1α and 2α peptides of the C-terminal oxygen-dependent degradation domain (CODD) that contains single target proline, which is thought to be predominant over the N-terminal oxygen-dependent degradation domain (NODD)[10]. PHD2 WT bound tightly to HIF1αCODD and HIF2αCODD peptides (7.5 and 15 μM, respectively). Notably, all but one tested PHD2 mutants (A228S, F366L and R371H) displayed mild binding defects, up to approximately 2-fold, to HIF1αCODD in comparison to WT PHD2 while P317R showed a severe binding defect with high K_d value (320 μM) (**Figure 4A** and **Table 2**). Similar pattern of binding deficiencies was noted for PHD2 mutants to HIF2αCODD (**Figure 4B** and **Table 2**), suggesting no significant preferential binding defects to either HIFα paralog.

NMR reveals major defect in PHD2 P317R-mediated hydroxylation of NODD proline

Previously, we developed an assay utilizing NMR to directly measure PHD2 hydroxylation of the critical two prolines located within the intrinsically disordered ODD of HIF1α[12]. Under the catalysis of PHD2, movement of resonances corresponding to the target prolines as well as adjacent residues are observed, reflecting local conformational changes due to the post-translational modification of HIF1αODD. The time-dependent shift in peak intensity from unhydroxylated to hydroxylated species can be interpreted as a function of the reaction progress. Notably, the

enzymatic kinetics of the hydroxylation of both target prolines (P402 in NODD, P564 in CODD) can be measured simultaneously over time by using the resonance movement of neighboring residues as reporters (A403 for NODD, I566 for CODD) (**Supplemental Figure 5**). Since binding experiments with PHD2 mutants did not implicate marked preferential defects for either HIF1α or HIF2α, these assays were performed with HIF1αODD of which more than 95% of amino acids have been assigned to their corresponding 3D NMR backbone cross-peak[12].

We selected PHD2 A228S for NMR study to determine if this mutant, which showed negligible to minute defect in the above studies from HRE-driven luciferase assay to MST based binding experiments, exhibited any appreciable enzymatic defect in hydroxylating P564 or P402. We included as controls PHD2 WT and P317R that showed major defect in binding HIF1αCODD peptide and transcriptional activation of HRE-luciferase. As shown previously[12], PHD2 WT showed robust and rapid hydroxylation of P564 in CODD and a markedly slower hydroxylation of P402 in NODD (**Figure 5A**). PHD2 A228S mutant effectively hydroxylated P564 faster than P402 with negligible differences in the enzymatic rate to PHD2 WT (**Figure 5A**). Unexpectedly, P317R displayed a near wild-type hydroxylation of P564 but failed to hydroxylate P402 (**Figure 5A**). Superimposition of ^{1}H-^{15}N HSQC spectra showed that cross-peak of P564 shifts with PHD2 WT, A228S, and P317R mutant, but P402 only shifts when incubated with PHD2 WT and A228S, not PHD2 P317R (**Figure 5B**). These results are inconsistent with observations made via MST that showed P317R having a severe binding defect for HIF1αCODD peptide. Furthermore, it is of particular interest to investigate whether the lack of activity of PHD2 P317R on NODD is due to a loss of binding interaction.

PHD2 P317R binds effectively to both CODD and NODD via BLI

We performed bio-layer interferometry (BLI) using immobilized biotinylated HIF1αCODD and NODD peptides with purified PHD2 WT and P317R, which showed P317R binding to CODD peptide only slightly weaker than PHD2 WT (**Table 3**). The discrepancy between the MST and BLI results may be due to the amine-linked fluorescent labelling of PHD2 P317R for MST, potentially disrupting binding to HIF1αCODD peptide. The removal of this label allowed for proper, unimpeded interaction to occur as observed with BLI. These results are consistent with the near-WT, efficient hydroxylation of HIF1αCODD by PHD2 P317R as revealed by NMR (See **Figure 5**).

The binding affinity between PHD2 P317R and HIF1αNODD was also measured to examine whether the catalytic defect observed via NMR would manifest as a binding defect. However,

PHD2 P317R bound to NODD similarly to PHD2 WT suggesting that its failure to hydroxylate P402 is unlikely attributable to binding. Binding between PHD2 WT and P317R with hydroxylated peptides was measured as a negative control, validating BLI as a viable technique for detecting binding defects (**Supplementary Figure 2**).

DISCUSSION

Mutations occurring in the core components of the hypoxia sensing pathway have been shown to cause various phenotypes ranging from erythrocytosis and neuroendocrine tumors to hemangioblastoma and renal cell carcinoma. Collectively, these diseases are referred to as pseudohypoxic diseases due to the inappropriate hypoxic response induced by the mutations. It is presumed that the abnormal response is the reason for overlapping phenotypes caused by mutations in different proteins of the same pathway (pVHL, HIF2α and PHD2). Specifically, we have proposed that the common phenotypes of pseudohypoxic diseases are caused by the gain-of-function ability of HIFα, in particular HIF2α, to escape degradation in the presence of the disease-causing mutants[31]. It has been shown that VHL disease-causing mutants have varying ability to target HIF1/2α for ubiquitin-mediated destruction[32,41] and Pacak-Zhuang syndrome-causing HIF2α mutants are able to escape recognition to a varying degree from both pVHL and PHD2[15,34]. It follows then that in the case of PHD2-driven erythrocytosis, PHD2 mutants would have a hindered ability to promote proper oxygen-dependent hydroxylation of HIF1α and 2α.

Complete deletion of PHD2 in mice causes embryonic lethality due venous congestion and cardiomyopathy, theorized to be directly related to high blood volume induced upon PHD2 loss[42]. Conditional inactivation of PHD2 whether globally[43] or in renal erythropoietin-producing cells[44] has been observed to cause erythrocytosis in mice. Moreover, while inactivation of PHD2 alone was sufficient to induce erythrocytosis, inactivating PHD1 or PHD3 alone did not result in erythrocytosis. However, when PHD1 or PHD3 were inactivated in addition to PHD2, erythrocytosis phenotype worsened, suggesting a supporting role for the PHD paralogs[45].

Here, we examined 7 disease-causing PHD2 mutations across the catalytic core, the most frequently mutated region within PHD2. G206C, W334R and H374R exhibited gross protein stability defects and were prone to severe aggregation, which precluded their purification necessary for further biophysical analyses. One of these mutants, H374R, is located at the catalytic site integral to the function of PHD2, which combined with the stability defect likely abrogated its ability to promote the oxygen-dependent hydroxylation of ectopic HIF1α, leading to

increased HRE-luciferase transcriptional activity in *PHD2-/-* HEK293A cells. Previous work has shown mutating analogous His iron-coordinating residues to a charged residue (Arg or Glu) in the prolyl-4-hydroxylase responsible for hydroxylating prolines of collagen abolishes enzymatic activity[46]. Given the high structural conservation in the Fe/2OG-oxygenase enzyme family[29], it can be predicted that a comparable mutation on PHD2 would also abolish activity. Structurally, G206 is located at a sharp turn in PHD2, requiring the flexibility afforded by glycine. This property may be difficult to substitute without detriment as is observed with G206C. W334 is in a loop that connects the beta strands making up the highly conserved jelly roll structure of 2OG oxygenases[29]. A mutation at W334 may impact the orientation of this loop and destabilize the structure of PHD2. Our data corroborates this theory by revealing W334R to be highly unstable in cells and *in vitro*. However, PHD2 G206C and W334R mutants showed similar capacity as the PHD2 WT to inhibit the transcriptional activity of ectopic HIF1α. This may have been due to the nature of transfected PHD2 in which mutant PHD2s that are prone to aggregation and instability are being translated throughout the luciferase assay, which may generate a small pool of monomeric PHDs that is sufficient to inhibit the transcriptional activity of HIF1α comparable to PHD2 WT.

The remaining four mutants (A228S, P317R, F366L, and R371H) not prone to aggregation displayed an overall structure similar to PHD2 WT, as determined by CD, and with the exception of PHD2 P317R (discussed later), were able to effectively suppress the ectopic HIF1α transcriptional activity. These mutants also exhibited slight thermal instability with mildly weaker binding affinity to HIF1αCODD peptide, which may be sufficient to cause the disease phenotype *in vivo*. PHD2 A228S exhibited the most minute of defects amongst all mutants tested and concordantly showed marginal reduction in enzymatic activity as measured via time-resolved NMR. Notably, despite these defects, albeit subtle, it is evident that the HRE-luciferase reporter assay is in general not reliable to reveal the disease-causing mutations on the functional output of PHD2 mutants, including those prone to aggregation (G206C and W334R). This represents a limitation in the interpretation of the HRE-luciferase reporter assay as mutants with clear structural defects do not necessarily impact downstream hypoxic signaling.

We recently developed a time-resolved NMR approach to directly and simultaneously measure PHD2-mediated hydroxylation of P564 within CODD and P402 within NODD in the context of full-length HIF1αODD. We showed that P564 is the predominant oxygen-dependent hydroxylation site over P402. Considering that pVHL only requires one hydroxylated proline for binding and triggering rapid ubiquitin-mediated proteasomal degradation of HIF1α[10-12,47], the

biological utility of P402 was thought to be inconsequential in normal hypoxic response. Here, our results revealed a previously unappreciated intricacy in the enzymatic selectivity of PHD2 P317R between CODD and NODD, challenging the current notion of NODD insignificance. NMR results showed that the disease-causing PHD2 P317R retained near-WT activity on CODD P564 but had negligible activity on NODD P402. Furthermore, despite effective activity on P564, ectopic PHD2 P317R generated abnormally high HRE-driven luciferase reporter signal, suggesting the negative impact of defective P402 hydroxylation on an otherwise rapid oxygen-dependent degradation of HIF1α. This is congruous with Schofield's earlier work that showed, using an indirect metabolic method with individual peptides, no activity on NODD by PHD2 P317R while effectively hydroxylating CODD[38]. Given the pathogenic nature of P317R mutation, it appears likely that this selective defect on HIF1αNODD contributes to the development of erythrocytosis and therefore, the involvement of NODD in normal oxygen-sensing pathway is not insignificant.

The molecular basis for PHD2 P317R's selective defect for NODD is currently unknown. Comparison of WT and P317R PHD2 crystal structures suggest that P317 makes hydrophobic contacts with the LXXLAP motif on HIFα and R317 may interact differently with this motif, impacting HIFα binding[38]. Intriguingly, BLI results showed that PHD2 P317R binds to both CODD and NODD peptides comparable to PHD2 WT. Substrates of Fe/2OG-oxygenases typically bind the enzymes non-covalently with a prime separation distance of 4-5 Å between the target atom and the catalytic iron[48]. One possibility is that the Pro to Arg substitution at position 317 may increase the distance between HIF1α P402 and the active site within the catalytic core without compromising the interaction between the substrate and enzyme. However, such mutation did not markedly impact the efficient turnover of P564, suggesting that the varied residues between NODD and CODD may influence the substrate selectivity of PHD2.

Some mutants, namely A228S and F366L, appear to be like PHD2 WT according to the tests performed. Minor binding and stability defects were observed with both mutants, yet it remains unclear if this is the pathogenetic mechanism. Upon structural review, it becomes clear that F366L would disrupt the hydrophobic core of PHD2, and this instability can be observed in the CHX assay but not in the other assays. An A228S-caused defect is less obvious. A228 is located on the surface of the catalytic core and while it is possible a residue change to polar serine could impact how PHD2 interacts in solution, this remains to be validated. This raises the notion that these mutants may have defects interacting with previously proposed though controversial alternate non-HIF substrates[49].

PHD2-driven erythrocytosis is a relatively newly discovered genetic disease with the first reported case in 2006. Since then, there has been a large increase in reports owing to the addition of *EGLN1* mutant screening in recent years for cases of idiopathic erythrocytosis[32]. As further awareness of the disease grows, screening will increase, leading to the likely identification of more disease-associated mutations. This study, therefore, will add to the groundwork knowledge of how mutant PHD2 induces disease in the context of the hypoxic response.

MATERIALS AND METHODS

Plasmids, antibodies, and peptides

Previously described plasmids were used as follows: pET-46-HIS$_6$-PHD2[15], pGL3-VEGFA-HRE[34], pCDF-Ek/LIC-StrepII-HIS$_6$-HIF1α ODD[12], pcDNA3-HA-HIF1α [10]. pRL-SV40 was procured from Promega. pcDNA3-3XFLAG-EGLN1 was generated by amplifying the EGLN1 gene from HA-EglN1-pcDNA3 (a gift from William Kaelin; Addgene plasmid # 18963) using primers 5' – GCG GCG GGA TCC ATG GCC AAT GAC AGC G – 3' and 5' – GCG GCG TCT AGA CTA GAA GAC GTC TTT ACC GAC – 3'. The product was digested with BamHI/XbaI and subcloned into pcDNA3 vector containing an N-terminal 3XFLAG tag. pX330-U6-Chimeric_CBh-hSpCas9 was gifted to the lab from Feng Zhang (Addgene plasmid #42230). PHD2 mutants of pET-46-HIS$_6$-PHD2 and pcDNA3-3XFLAG-PHD2 were generated through QuikChange site directed mutagenesis (Agilent). Mutant sequences were confirmed via DNA sequencing. The following antibodies were used: α-HA (C29F4) from Cell Signaling, α-FLAG M2 (F1804) from Sigma-Aldrich, α-Vinculin (V9264) from Sigma-Aldrich, α-HIF1α (36169) from Cell Signaling, and α-PHD2/EGLN1 (D31E11) from Cell Signaling. Primary antibodies were diluted in TBS-T (20 mM Tris pH 7.6, 137 mM NaCl, 0.05% (v/v) Tween 20) with 0.02% (w/v) sodium azide for immunoblotting. Peptides were N-terminally acetylated for microscale thermophoresis (MST) and biotinylated for bio-layer interferometry (BLI). All peptides were amidated at the C-terminus. For microscale thermophoresis, peptides were reconstituted in 50mM Tris (tris(hydroxymethyl)aminomethane) pH 8.0 buffer. For bio-layer interferometry, peptides were reconstituted in 100% (v/v) DMSO.

PHD2 -/- HEK293A Cells

Wild-type (WT) human epithelial kidney (HEK293A) cells were subjected to the clustered regularly interspaces short palindromic repeats (CRISPR) method to generate homozygous PHD2 knockout (-/-) cells. The CRISPOR design tool was used to generate CRISPR guide RNAs (gRNA) targeting

exon 1 in *EGLN1*[50]. Forward and reverse gRNA oligonucleotides were phosphorylated and annealed before ligation into *BbsI*-digested pX330-U6-Chimeric_CBh-hSpCas9. WT HEK293A cells were transfected with pX330-EGLN1 gRNA using Lipofectamine 2000 according to manufacturer instructions. Single cell colonies were seeded into 96-well plates from the previously transfected cells at a density of 1.25 cells/mL. 200 μl of cells were seeded into each well resulting in a density of ~0.25 cells/well. Single cell clones were screened for PHD2 knockout via immunoblotting for PHD2. Western blots validating PHD2 knockout are shown in Supplementary Information (**Supplementary Figure 4**).

Dual Luciferase Assay

A dual luciferase assay was performed according to a modified previously reported protocol[34]. PHD2 -/- HEK293A cells were grown and maintained in Dulbecco's Modified Eagle Medium (DMEM, Wisent) with 10% (v/v) Fetal Bovine Serum (FBS, Wisent) and 100 IU/mL penicillin and streptomycin in a humidified incubator at 37°C and 5% CO_2. Transfection complexes consisted of 2 μg total DNA: 0.4 μg pcDNA3-HA, 0.9 μg pGL3-VEGFa-HRE, 0.1 μg pRL-SV40, 0.4 μg pcDNA3-HA- HIF1α, and 0.2 μg pcDNA3-FLAG3X-PHD2 (WT or mutant). Complexes were incubated for 15 minutes at room temperature with 8 μg polyethleneimine pH 7.2 (Polysciences) in 400 ml of OptiMEM™ Reduced Serum Media (Gibco). Following incubation, transfection complexes were added to 5 x 10^5 PHD2-/- HEK293A cells suspended in 400 μl OptiMEM™ and incubated for 5 minutes. Cells were transferred to six well plates and incubated at 37°C, 5% CO_2 for 24 hours. Cells were lysed and processed according to the Promega Dual-Luciferase Reporter Assay System (#E1960) instructions. Firefly luciferase and Renilla luciferase activity were measured on a Varioskan Lux microplate reader (Thermo Fisher Scientific). Luciferase activity was normalized by dividing Firefly RLU values by the constitutively expressed, control Renilla RLU values. Normalized RLU values were transformed by setting the RLU value of the WT PHD2 sample to 1 and dividing the other sample values by the same transformation factor. A two-tailed t-test was performed to determine statistically significant differences between samples. A p-value below 0.0332 was considered significant. Protein levels of PHD2 were determined by immunoblotting for FLAG3X-PHD2. Vinculin was probed as a loading control.

Cycloheximide Chase Assay

HEK293A cells were cultured as described above. Transfection complexes consisting of 1.5 μg total DNA were incubated with 6 μg Polyethyleneimine pH 7.2 in 400 μl of OptiMEM™ for 15 min at room temperature. Transfection complexes consisted of either 0.5 μg (WT, A228S, P317R, F366L, R371H) or 1.5 μg (G206C, W334R, H374R) of pcDNA3-FLAG3X-PHD2. Additional pcDNA3-FLAG3X-PHD2 was transfected for less stable mutants to ensure equal amounts of PHD2 expression. The total amount of DNA was brought to 1.5 μg with the addition of 1 μg of pcDNA3 if necessary. Transfection complexes were added to 1.5 x 10^5 cells suspended in 400 μl OptiMEM™ and incubated for 5 minutes. Cells were plated in 60 mm plates with 5 plates for each mutant and 2 for WT. Cells were incubated for 24 hours at 37°C and 5% CO_2. Following incubation, media was replaced to remove Polyethyleneimine and fresh media with 10 μg/ml cycloheximide (CHX) was added. Cells were incubated in CHX supplemented media for 0, 3, 6, 12 and 24 hours. WT samples were incubated only for 0 and 24 hours. Cells were harvested through manual scraping and lysed via sonication in 250 μl of cold EBC lysis buffer (50 mM Tris, 120 mM NaCl, 0.5% (v/v) NP-40) supplemented with 1X protease inhibitor cocktail (BioShop PIC002.1). Protein levels were determined via Bradford assay and equal protein amounts of lysate were denatured by boiling for 5 minutes with 3X sample buffer (62.5 mM Tris, 10% (v/v) glycerol, 2% (w/v) SDS, 0.01% (w/v) bromophenol blue). Samples were then resolved on a 10% acrylamide SDS-PAGE gel for 90 minutes at 120 V. Proteins were transferred to polyvinylidene fluoride (PVDF) membrane via wet electrophoretic transfer for 70 minutes at 110 V. Membranes were blocked for 60 minutes at room temperature in 5% (w/v) skim milk in TBS-T. Membranes were then incubated with α-FLAG-M2 (1:1500) and α-vinculin (1:1500) at 4°C overnight. Following three washes with TBS-T, membranes were incubated with HRP-conjugated secondary antibodies (1:10,000 in 5% (v/v) skim milk in TBS-T) for 60 minutes at room temperature. Proteins were detected using a chemiluminescence solution and imaged with a ChemiDoc™ MP Imaging System (BioRad). Immunoblot band density was quantified using BioRad Image Lab densitometry software. FLAG3X-PHD2 levels were normalized according to corresponding vinculin levels. Each 0-hour sample was set to 1 and each other time point was divided by this value to reflect relative protein levels. A two-tailed t-test was performed to identify significant differences between 0 hour and 24-hour timepoints. A p-value below 0.0332 was considered significant.

PHD2 (181-426) Expression and Purification

BL21 (DE3) *E. coli* cells (Novagen, #69450) were transformed with pET-46-HIS$_6$-PHD2 (wild type or mutant). 1 liter Luria Broth (LB) cell cultures were grown at 37°C until OD_{600} reached ~0.8. Cultures were then induced with a final concentration of 1 mM Isopropyl ß-D-1-thiogalactopyranoside (IPTG) for 16 hours at 16°C. Cultures were harvested via centrifugation and stored at -80°C for future use. His$_6$-PHD2 (181-426) was purified according to a previously described protocol[51]. Bacterial pellets were resuspended in lysis buffer (50 mM Tris-HCl pH 7.9, 500 mM NaCl, 5 mM imidazole) supplemented with 1X SigmaFast protease inhibitor cocktail (Sigma-Aldrich). Cells were lysed with 3 passes through a cell disruptor at 30 kpsi. Cell lysate was cleared via centrifugation at 30,000 g for 45 minutes. Cleared lysates were applied to a 2 mL Ni-NTA resin (ThermoFisher). The resin was washed with 10 mL of lysis buffer followed by 2 separate 30 mL washes with Wash buffer (50 mM Tris-HCl pH 7.9, 500 mM NaCl, 30 mM imidazole). His$_6$-PHD2 was eluted from the resin with 10 mL of elution buffer (50 mM Tris-HCl pH 7.9, 500 mM NaCl, 1 M imidazole). The eluate was dialyzed against 2 liters of dialysis buffer (50 mM Tris-HCl pH 7.5) using a 10 kDa cut-off dialysis membrane. After 4 hours, the dialysis buffer was replaced with 2 fresh liters and 1.5 units of thrombin was added per mg of His$_6$-PHD2. His$_6$-PHD2 was dialyzed overnight with thrombin at 4°C. The dialyzed PHD2 was applied to Ni-NTA resin equilibrated with dialysis buffer to separate thrombin-cleaved protein from uncleaved protein and His$_6$ tags. The resin was washed with dialysis buffer supplemented with 5 mM imidazole. The flowthrough and wash were combined and concentrated to ~600 µl using an Amicon 10 kDa cut-off centrifugal concentrator (Millipore). The concentrated PHD2 was cleared at 13,000 rpm for 10 minutes then applied to a Superdex™ 200 Increase 10/300 (Cytiva) column equilibrated with dialysis buffer or labeling buffer (50 mM HEPES (N-2-hydroxyethylpiperazine-N'-2-ethanesulfonic acid) pH 7.5, 150 mM NaCl). Elution was monitored via UV absorbance and samples with PHD2 were collected. SDS-PAGE gels were run to confirm purity. PHD2 proteins were concentrated to > 2 mg/ml. The final concentration was measured via UV absorbance at 280 nm ($\varepsilon_{0.1\%}$ = 1.34). Unlabeled protein was flash frozen and stored at -80°C for use in circular dichroism and nuclear magnetic resonance. For size exclusion column analysis, the protein was concentrated to around 2 mg/ml prior to application to the Superdex™ 200 Increase 10/300 (Cytiva) column and the His6 tag was not cleaved.

PHD2 proteins used for microscale thermophoresis (MST) were labelled with Alexa Fluor-647 N-hydroxylsuccinimide ester dye (Thermo Scientific) following purification according to a previously reported protocol[34]. PHD2 proteins were diluted to 1 mg/ml and Alexa Fluor-647 dye was added to 500 µl of protein in a 4:1 molar ratio (dye: PHD2). Following incubation at room

temperature in the dark for 1-hour, excess dye was removed using a PD-10 Sephadex™ G-25 M desalting column (Cytiva) equilibrated with dialysis buffer. Labelled protein subjected to a 10-fold dilution in dialysis buffer and was then concentrated using a 10 kDa cut-off Amicon centrifugal concentrator to remove excess dye. Alexa Fluor-647 labelled PHD2 was then brought to 10 mM in dialysis buffer, flash frozen and stored at -80°C for use in MST.

HIF1α ODD (394-574) Expression and Purification

DNA corresponding to the sequence of human HIF-1α ODD (residue 394-574) with a C-terminal Strep Tag II (WSHPQFEK) was cloned into a pCDF Ek/LIC vector (EMD Millipore). Thrombin cleavage sites were included after the N-terminal-His_6 tag and before the C-terminal Strep Tag II. HIF-1α ODD was expressed in Rosetta-2 (DE3) cells. To produce ^{15}N-labeled proteins, cells were grown in 2X M9 minimal media, supplemented with a final concentration of 1 g/L $^{15}NH_4Cl$ (ACP chemicals) and 4 g/L D-glucose (Bioshop). Expression and purification of HIF-1α ODD was previously described[12]. Briefly, cleared lysate was applied to Ni-NTA resin (ThermoFisher) and eluted with 300 mM imidazole. The elution was then incubated with StrepTactin XT 4Flow resin (IBA Lifesciences) overnight. Protein was eluted from the StrepTactin resin with 50 mM biotin. This process was repeated with the flowthrough from the StrepTactin beads to capture remaining unbound protein. Protein was concentrated and run on a Bio-Rad SEC650 10/300 column. Fractions containing HIF-1α ODD were then run on a HiResQ 5/50 (Cytiva) anion exchange column. After tag cleavage with thrombin, purified HIF-1α ODD was concentrated to 0.9 mM and stored at -80°C for future use.

Circular Dichroism

Purified PHD2 proteins were buffer exchanged on PD-10 Sephadex™ G-25 M desalting columns (Cytiva) for 5 mM KH_2PO_4/K_2HPO_4 pH 7.4 buffer. Proteins were then diluted to 0.1 mg/ml. Far-UV wavelength scans were collected from 190-260 nm on a Jasco-J-1500 CD spectrophotometer with a 1-mm pathlength quartz cuvette (Helma). CD values were averaged from 20 accumulations, baseline buffer subtracted and converted into mean residue ellipticity (degrees cm^2 $dmol^{-1}$). Spectra were smoothed using Jasco Spectra Analysis software. Wavelength scans were run in triplicate and the average mean residue ellipticity was plotted with other PHD2 CD curves.

Melting curves were generated by monitoring CD values for each PHD2 protein from 25-95°C at 220 nm with 1°C steps. Values were baseline buffer subtracted and converted to mean

residue ellipticity. Triplicate non-transformed data was plotted. Curves were transformed by setting the average peak value between 25-37°C to 1.0 and normalizing other points according to the same normalization factor. Curves were fitted with a sigmoidal curve on Prism. Corresponding R^2 values are recorded in Table 1. Melting temperature (T_m) for each protein were determined from the EC50 of each sigmoidal curve. Curves were plotted using GraphPad Prism version 10.2.3.

Microscale Thermophoresis

Microscale Thermophoresis (MST) binding tests and analysis were performed according to a previously recorded protocol[34]. A Monolith NT.115 (Nanotemper Technologies) was used at room temperature to record MST measurements. 2X stock solutions of Alexa Fluor-647-labeled PHD2 with necessary hydroxylation reagents was made (50 nM Alexa Fluor-647-PHD2, 50 mM Tris-HCl pH 7.5, 1 mM N-oxalylglycine (NOG), 10 μM ferrous sulfate, 5 mg/ml BSA). ~1 mg lyophilized HIF1α $_{555-574}$ CODD and HIF2α $_{522-542}$ CODD peptides were dissolved in 200 μl of 50 mM Tris HCl pH 8.0 and their concentrations were measured via UV absorbance with the following extinction coefficient: 1490 M^{-1} cm^{-1}. Starting with the stock HIFα peptide solutions, two-fold serial dilutions were performed to generate 16 different 15 μl HIFα concentrated solutions. 15 μl of 2X Alexa-647-PHD2 solution was then added to each HIFα peptide dilution resulting in a final Alexa-647-PHD2 concentration of 25 nM. The solutions were incubated at room temperature for 10 minutes then loaded into standard MST capillaries (Nanotemper Technologies). MST measurements were recorded using 20% fluorescence excitation LED power and 40% (medium) infrared (IR) laser power. Measurements were recorded for 5 seconds prior to IR laser activation, 20 seconds during IR activation and 3 seconds following IR deactivation. The experimental data was analyzed and fit with a 1:1 K_d binding model using M.O. affinity analysis software (Nanotemper Technologies). Curves were plotted on GraphPad Prism (version 10.2.3).

Bio-layer Interferometry

The binding affinities of HIF1α peptides and WT or P317R PHD2 were measured by bio-layer interferometry (BLI) using a single channel BLItz instrument (Sartorius). Purified PHD2 was concentrated to 0.45 mM and diluted into BLI Kinetic Buffer (20 mM Tris-HCl pH 7.4, 100 mM NaCl, 1 mM L-ascorbic acid (Sigma), 100 μM ferrous chloride tetrahydrate (Sigma), 1 mM N-oxalylglycine (Sigma), 0.1% (w/v) Bovine Serum Albumin and 0.1% (v/v) Tween-20). Following reconstitution to a final concentration of 2 mg/ml in DMSO, biotinylated HIF1α peptides were diluted 200-fold in the

BLI Kinetic Buffer. HIF1α peptides were immobilized on a streptavidin-coated biosensor (Sartorius) for 120 seconds before measuring association to WT PHD2 or P317R PHD2 in a concentration series over 120 seconds. Subsequently, the biosensor was immersed in the BLI Kinetic Buffer for 120 seconds to measure dissociation of the analyte. The sensorgrams were referenced and step corrected, and the binding affinities and kinetic rates were calculated based on global fit of the data to a 1:1 binding model using the BLItz Pro v.1.3.0.5 software. All binding measurements were performed in technical triplicates.

Real-time Prolyl-hydroxylation Kinetic Measurement

Real-time prolyl hydroxylation of HIF1α ODD was measured according to a previously reported protocol based on Nuclear Magnetic Resonance (NMR)[12]. NMR experiments were performed at the UHN Nuclear Magnetic Resonance Core Facility on a Bruker 800 MHz US2 equipped with a NEO console and a 5 mm triple-resonance ^{13}C optimized TXO cryoprobe, Z-gradient. NMR samples were prepared in 50 mM Tris-HCl pH 7.5, 100 mM NaCl, and 0.5 mM Tris(2-carboxyethyl) phosphine hydrochloride (TCEP-HCl) (NMR buffer) supplemented with 5% D_2O. Prior to the experiments, NMR buffer was gassed with 99.6% oxygen (Messer) for 40 minutes and then used to dilute 0.9 mM of HIF1α ODD to a final concentration of 0.18 mM. Samples were transferred to a 5-mm NMR tube pre-purged with 99.6% oxygen for 10 minutes. The real-time hydroxylation experiments were conducted at 25°C using the ^{1}H-^{15}N HSQC pulse sequence with sodium 2,2-dimethyl-2-silapentane-5-sulfonate (DSS) as reference. For each experiment, a ^{1}H-^{15}N HSQC spectrum of HIF1α ODD was acquired prior to initiating the hydroxylation reaction with the addition of purified WT or mutant PHD2 at a molar ratio of 1:20 versus HIF1α ODD with 5 mM α-ketoglutaric acid disodium salt dihydrate (Sigma), 2 mM L-ascorbic acid (Sigma), and 0.1 mM ferrous chloride tetrahydrate. Multiple ^{1}H-^{15}N HSQC spectra with acquisition time of 602 seconds were acquired over the course of 20.18 hours. After 6 consecutive acquisitions of ^{1}H-^{15}N HSQC spectra, the subsequent spectra were acquired with interscan delays of 2400 seconds. Kinetic measurements with WT, A228S, and P317R PHD2 were performed in technical duplicates.

Real-time hydroxylation of P402 and P564 of HIF1 α was measured by monitoring resonance shifting of A403 and I566[12] respectively, in all ^{1}H-^{15}N HSQC spectra. Both resonances shifted as reflections of changes in the local chemical environments upon prolyl-hydroxylation. Reaction progress was reported as the peak intensity of the shifted resonance over the sum of peak intensities for both shifted and unshifted resonances. All spectra were processed with the

NMRPipe software[52] and analyzed using the CcpNmr Version-3 software[53]. Kinetic curves were plotted using GraphPad Prism (version 10.2.3).

ACKNOWLEDGEMENTS

We thank the members of the Lee and Ohh labs for their critical comments and helpful discussions. This study was supported by funds from the Canadian Institutes of Health Research (MOP-133694 to J.E.L. and PJT-191811 to M.O.) and the generous donations from Colorworks Canada (to M.O.). The UHN NMR Core Facility was supported by the Princess Margaret Cancer Foundation. Infrastructure for biophysics and NMR was funded by the Canada Foundation for Innovation (CFI).

AUTHOR CONTRIBUTIONS

C.C.T. designed and performed the experiments, interpreted the data, and wrote the manuscript. W. H. performed the Bio-layer interferometry. W.H. and G.M.C.G.-S. performed the real time Prolyl-hydroxylation assay. M.H. assisted in performing the CHX chase assays. C.C.T., F.G.F, and M.O. conceptualized the project. G.M.C.G.-S., M.I., and J.E.L. contributed new reagents and analytical tools. M.O. interpreted the data, wrote and edited the manuscript. All authors reviewed and edited the manuscript.

CONFLICT OF INTEREST DISCLOSURES

The authors declare no potential conflicts of interest.

REFERENCES:

1 Lee, F. S. & Percy, M. J. The HIF pathway and erythrocytosis. *Annu Rev Pathol* **6**, 165-192 (2011). https://doi.org:10.1146/annurev-pathol-011110-130321

2 Weidemann, A. *et al*. The glial cell response is an essential component of hypoxia-induced erythropoiesis in mice. *J Clin Invest* **119**, 3373-3383 (2009). https://doi.org:10.1172/JCI39378

3 Richmond, T. D., Chohan, M. & Barber, D. L. Turning cells red: signal transduction mediated by erythropoietin. *Trends Cell Biol* **15**, 146-155 (2005). https://doi.org:10.1016/j.tcb.2005.01.007

4 Bhoopalan, S. V., Huang, L. J. & Weiss, M. J. Erythropoietin regulation of red blood cell production: from bench to bedside and back. *F1000Res* **9** (2020). https://doi.org:10.12688/f1000research.26648.1

5 Semenza, G. L. & Wang, G. L. A nuclear factor induced by hypoxia via de novo protein synthesis binds to the human erythropoietin gene enhancer at a site required for

transcriptional activation. *Mol Cell Biol* **12**, 5447-5454 (1992). https://doi.org:10.1128/mcb.12.12.5447-5454.1992

6 Mithoowani, S., Laureano, M., Crowther, M. A. & Hillis, C. M. Investigation and management of erythrocytosis. *CMAJ* **192**, E913-E918 (2020). https://doi.org:10.1503/cmaj.191587

7 Lippl, K. *et al.* Born to sense: biophysical analyses of the oxygen sensing prolyl hydroxylase from the simplest animal Trichoplax adhaerens. *Hypoxia (Auckl)* **6**, 57-71 (2018). https://doi.org:10.2147/HP.S174655

8 Dengler, V. L., Galbraith, M. & Espinosa, J. M. Transcriptional regulation by hypoxia inducible factors. *Crit Rev Biochem Mol Biol* **49**, 1-15 (2014). https://doi.org:10.3109/10409238.2013.838205

9 Schodel, J. *et al.* High-resolution genome-wide mapping of HIF-binding sites by ChIP-seq. *Blood* **117**, e207-217 (2011). https://doi.org:10.1182/blood-2010-10-314427

10 He, W., Batty-Stuart, S., Lee, J. E. & Ohh, M. HIF-1alpha Hydroxyprolines Modulate Oxygen-Dependent Protein Stability Via Single VHL Interface With Comparable Effect on Ubiquitination Rate. *J Mol Biol* **433**, 167244 (2021). https://doi.org:10.1016/j.jmb.2021.167244

11 Chan, D. A., Sutphin, P. D., Yen, S. E. & Giaccia, A. J. Coordinate regulation of the oxygen-dependent degradation domains of hypoxia-inducible factor 1 alpha. *Mol Cell Biol* **25**, 6415-6426 (2005). https://doi.org:10.1128/MCB.25.15.6415-6426.2005

12 He, W., Gasmi-Seabrook, G. M. C., Ikura, M., Lee, J. E. & Ohh, M. Time-resolved NMR detection of prolyl-hydroxylation in intrinsically disordered region of HIF-1alpha. *Proc Natl Acad Sci U S A* **121**, e2408104121 (2024). https://doi.org:10.1073/pnas.2408104121

13 Clifford, S. C. & Maher, E. R. Von Hippel-Lindau disease: clinical and molecular perspectives. *Adv Cancer Res* **82**, 85-105 (2001). https://doi.org:10.1016/s0065-230x(01)82003-0

14 Neumann, H. P. & Wiestler, O. D. Clustering of features and genetics of von Hippel-Lindau syndrome. *Lancet* **338**, 258 (1991). https://doi.org:10.1016/0140-6736(91)90401-a

15 Tarade, D., Robinson, C. M., Lee, J. E. & Ohh, M. HIF-2alpha-pVHL complex reveals broad genotype-phenotype correlations in HIF-2alpha-driven disease. *Nat Commun* **9**, 3359 (2018). https://doi.org:10.1038/s41467-018-05554-1

16 Pacak, K. *et al.* New syndrome of paraganglioma and somatostatinoma associated with polycythemia. *J Clin Oncol* **31**, 1690-1698 (2013). https://doi.org:10.1200/JCO.2012.47.1912

17 Pacak, K. *et al.* Ocular manifestations of hypoxia-inducible factor-2alpha paraganglioma-somatostatinoma-polycythemia syndrome. *Ophthalmology* **121**, 2291-2293 (2014). https://doi.org:10.1016/j.ophtha.2014.06.019

18 Delamare, M. *et al.* Characterization of genetic variants in the EGLN1/PHD2 gene identified in a European collection of patients with erythrocytosis. *Haematologica* **108**, 3068-3085 (2023). https://doi.org:10.3324/haematol.2023.282913

19 Gardie, B. *et al.* The role of PHD2 mutations in the pathogenesis of erythrocytosis. *Hypoxia (Auckl)* **2**, 71-90 (2014). https://doi.org:10.2147/HP.S54455

20 Yang, C. *et al.* Germ-line PHD1 and PHD2 mutations detected in patients with pheochromocytoma/paraganglioma-polycythemia. *J Mol Med (Berl)* **93**, 93-104 (2015). https://doi.org:10.1007/s00109-014-1205-7

21 Percy, M. J. *et al.* A family with erythrocytosis establishes a role for prolyl hydroxylase domain protein 2 in oxygen homeostasis. *Proc Natl Acad Sci U S A* **103**, 654-659 (2006). https://doi.org:10.1073/pnas.0508423103

22 Provenzano, A. *et al.* Novel Germline PHD2 Variant in a Metastatic Pheochromocytoma and Chronic Myeloid Leukemia, but in the Absence of Polycythemia. *Medicina (Kaunas)* **58** (2022). https://doi.org:10.3390/medicina58081113
23 Ladroue, C. *et al.* PHD2 mutation and congenital erythrocytosis with paraganglioma. *N Engl J Med* **359**, 2685-2692 (2008). https://doi.org:10.1056/NEJMoa0806277
24 Lenders, J. W., Eisenhofer, G., Mannelli, M. & Pacak, K. Phaeochromocytoma. *Lancet* **366**, 665-675 (2005). https://doi.org:10.1016/S0140-6736(05)67139-5
25 Berra, E. *et al.* HIF prolyl-hydroxylase 2 is the key oxygen sensor setting low steady-state levels of HIF-1alpha in normoxia. *EMBO J* **22**, 4082-4090 (2003). https://doi.org:10.1093/emboj/cdg392
26 Appelhoff, R. J. *et al.* Differential function of the prolyl hydroxylases PHD1, PHD2, and PHD3 in the regulation of hypoxia-inducible factor. *J Biol Chem* **279**, 38458-38465 (2004). https://doi.org:10.1074/jbc.M406026200
27 Flashman, E. *et al.* Kinetic rationale for selectivity toward N- and C-terminal oxygen-dependent degradation domain substrates mediated by a loop region of hypoxia-inducible factor prolyl hydroxylases. *J Biol Chem* **283**, 3808-3815 (2008). https://doi.org:10.1074/jbc.M707411200
28 Schofield, C. J. & Ratcliffe, P. J. Oxygen sensing by HIF hydroxylases. *Nat Rev Mol Cell Biol* **5**, 343-354 (2004). https://doi.org:10.1038/nrm1366
29 Clifton, I. J. *et al.* Structural studies on 2-oxoglutarate oxygenases and related double-stranded beta-helix fold proteins. *J Inorg Biochem* **100**, 644-669 (2006). https://doi.org:10.1016/j.jinorgbio.2006.01.024
30 Figg, W. D., Jr. *et al.* Structural basis for binding of the renal carcinoma target hypoxia-inducible factor 2alpha to prolyl hydroxylase domain 2. *Proteins* **91**, 1510-1524 (2023). https://doi.org:10.1002/prot.26541
31 Ohh, M., Taber, C. C., Ferens, F. G. & Tarade, D. Hypoxia-inducible factor underlies von Hippel-Lindau disease stigmata. *Elife* **11** (2022). https://doi.org:10.7554/eLife.80774
32 Rechsteiner, M. P. *et al.* VHL gene mutations and their effects on hypoxia inducible factor HIFalpha: identification of potential driver and passenger mutations. *Cancer Res* **71**, 5500-5511 (2011). https://doi.org:10.1158/0008-5472.CAN-11-0757
33 Maher, E. R. & Kaelin, W. G., Jr. von Hippel-Lindau disease. *Medicine (Baltimore)* **76**, 381-391 (1997). https://doi.org:10.1097/00005792-199711000-00001
34 Ferens, F. G. *et al.* Deficiency in PHD2-mediated hydroxylation of HIF2alpha underlies Pacak-Zhuang syndrome. *Commun Biol* **7**, 240 (2024). https://doi.org:10.1038/s42003-024-05904-4
35 Song, D. *et al.* Defective Tibetan PHD2 binding to p23 links high altitude adaption to altered oxygen sensing. *J Biol Chem* **289**, 14656-14665 (2014). https://doi.org:10.1074/jbc.M113.541227
36 Xiang, K. *et al.* Identification of a Tibetan-specific mutation in the hypoxic gene EGLN1 and its contribution to high-altitude adaptation. *Mol Biol Evol* **30**, 1889-1898 (2013). https://doi.org:10.1093/molbev/mst090
37 Arsenault, P. R. *et al.* A knock-in mouse model of human PHD2 gene-associated erythrocytosis establishes a haploinsufficiency mechanism. *J Biol Chem* **288**, 33571-33584 (2013). https://doi.org:10.1074/jbc.M113.482364
38 Chowdhury, R. *et al.* Structural basis for oxygen degradation domain selectivity of the HIF prolyl hydroxylases. *Nat Commun* **7**, 12673 (2016). https://doi.org:10.1038/ncomms12673

39 McDonough, M. A. *et al.* Cellular oxygen sensing: Crystal structure of hypoxia-inducible factor prolyl hydroxylase (PHD2). *Proc Natl Acad Sci U S A* **103**, 9814-9819 (2006). https://doi.org:10.1073/pnas.0601283103
40 Greenfield, N. J. Using circular dichroism spectra to estimate protein secondary structure. *Nat Protoc* **1**, 2876-2890 (2006). https://doi.org:10.1038/nprot.2006.202
41 Knauth, K., Cartwright, E., Freund, S., Bycroft, M. & Buchberger, A. VHL mutations linked to type 2C von Hippel-Lindau disease cause extensive structural perturbations in pVHL. *J Biol Chem* **284**, 10514-10522 (2009). https://doi.org:10.1074/jbc.M809056200
42 Minamishima, Y. A. *et al.* Somatic inactivation of the PHD2 prolyl hydroxylase causes polycythemia and congestive heart failure. *Blood* **111**, 3236-3244 (2008). https://doi.org:10.1182/blood-2007-10-117812
43 Li, X., Sutherland, S., Takeda, K., Fong, G. H. & Lee, F. S. Integrity of the prolyl hydroxylase domain protein 2:erythropoietin pathway in aging mice. *Blood Cells Mol Dis* **45**, 9-19 (2010). https://doi.org:10.1016/j.bcmd.2010.03.003
44 Franke, K. *et al.* HIF-1alpha is a protective factor in conditional PHD2-deficient mice suffering from severe HIF-2alpha-induced excessive erythropoiesis. *Blood* **121**, 1436-1445 (2013). https://doi.org:10.1182/blood-2012-08-449181
45 Takeda, K. *et al.* Regulation of adult erythropoiesis by prolyl hydroxylase domain proteins. *Blood* **111**, 3229-3235 (2008). https://doi.org:10.1182/blood-2007-09-114561
46 Myllyharju, J. & Kivirikko, K. I. Characterization of the iron- and 2-oxoglutarate-binding sites of human prolyl 4-hydroxylase. *EMBO J* **16**, 1173-1180 (1997). https://doi.org:10.1093/emboj/16.6.1173
47 Tian, Y. M. *et al.* Differential sensitivity of hypoxia inducible factor hydroxylation sites to hypoxia and hydroxylase inhibitors. *J Biol Chem* **286**, 13041-13051 (2011). https://doi.org:10.1074/jbc.M110.211110
48 Aik, W., McDonough, M. A., Thalhammer, A., Chowdhury, R. & Schofield, C. J. Role of the jelly-roll fold in substrate binding by 2-oxoglutarate oxygenases. *Curr Opin Struct Biol* **22**, 691-700 (2012). https://doi.org:10.1016/j.sbi.2012.10.001
49 Cockman, M. E. *et al.* Lack of activity of recombinant HIF prolyl hydroxylases (PHDs) on reported non-HIF substrates. *Elife* **8**, e46490 (2019).
50 Concordet, J. P. & Haeussler, M. CRISPOR: intuitive guide selection for CRISPR/Cas9 genome editing experiments and screens. *Nucleic Acids Res* **46**, W242-W245 (2018). https://doi.org:10.1093/nar/gky354
51 Hewitson, K. S., Schofield, C. J. & Ratcliffe, P. J. Hypoxia-inducible factor prolyl-hydroxylase: purification and assays of PHD2. *Methods Enzymol* **435**, 25-42 (2007). https://doi.org:10.1016/S0076-6879(07)35002-7
52 Delaglio, F. *et al.* NMRPipe: a multidimensional spectral processing system based on UNIX pipes. *J Biomol NMR* **6**, 277-293 (1995). https://doi.org:10.1007/BF00197809
53 Skinner, S. P. *et al.* CcpNmr AnalysisAssign: a flexible platform for integrated NMR analysis. *J Biomol NMR* **66**, 111-124 (2016). https://doi.org:10.1007/s10858-016-0060-y

FIGURE LEGENDS

Figure 1. Analysis of disease causing PHD2 mutants. (A) Distribution of mutation type calculated from clinical case reports. Case reports have been compiled and summarized in the supplementary information (B) Linear map of mutant location and frequency on PHD2. The zinc finger is comprised of residues 21-58 while the catalytic core ranges from 181-426. Each dot represents a clinical report of a disease-causing mutation at the given residue. Mutations selected for analysis have been highlighted in red. (C) Structure of PHD2 HIF1αCODD complex (PDB:5L9B) with PHD2 mutant locations highlighted (yellow). PHD2 (grey) and HIF1αCODD (red) are depicted as ribbons. PHD2 mutants selected for analysis are highlighted in green and labelled. The structure was turned 260° on the y-axis to highlight all mutant locations.

Figure 2. Methods in HEK293A cells detect defects in some PHD2 mutants but not all. (A) Dual luciferase reporter assays were performed to measure HIF1α transcriptional activity in the presence of PHD2 mutants in PHD2 -/- HEK293A cells. Individual data points are plotted. Loading accuracy was evaluated via immunoblotting for FLAG-tagged PHD2 and vinculin. (B) PHD2 mutant stability was measured via cycloheximide chase assay. HEK293A cells were transfected with wild type or mutant PHD2 constructs, with the amount of transfected adjusted to ensure equal expression at 0 hours. After 24 hours, the transfected cells were treated with CHX to halt protein production and monitor the stability of PHD2. Cells were harvested at various time points up to 24 hours and lysates were immunoblotted to measure PHD2 levels. (C) FLAG immunoblot density was quantified at each time point and normalized with vinculin density to yield a relative density. 24-hour time points were compared to determine significance. For A and C, bars represent mean values, and standard error is represented by error bars. * indicates $P < 0.0332$, ** indicates $P < 0.0021$, *** indicates $P < 0.0002$, and **** indicates $P < 0.0001$ (two-tailed t-test).

Figure 3. PHD2 mutants display instability through aggregation and decreased thermostability. (A) Chromatograms of PHD2 catalytic cores were acquired via SEC on a Superdex200 column. Curves have been normalized according to molecular concentrations. Dashed red lines indicate mutants that were not purified. n = 2 (B) CD was performed on PHD2 mutants to predict secondary structure variations. The far-UV spectra (190-260 nm) of the purified catalytic cores was measured and converted to molar ellipticity. (C) Molar ellipticity of PHD2 mutants was monitored at 220 nm from 25 to 95 °C to evaluate thermal stability. Melting curves were generated from the CD melt. Molar ellipticity values were normalized and transformed into a fraction of folded protein and fitted with a sigmoidal curve. Melting temperatures (T_m) were determined using the EC50 of each curve. T_m and R_2 are listed in **Table 1**.

Figure 4. PHD2 mutants have minor binding defects to HIF1α peptides. Microscale thermophoresis was performed on fluorescently labelled PHD2 and HIF1α 555-574 CODD (A) or HIF2α 522-542 CODD (B) peptides. PHD2 P317R displayed a severe binding defect whereas the other three mutants had minor binding defects. It is suspected that amine reactive fluorescent labelling induced a binding defect on PHD2 P317R. K_d values with standard deviation are listed in **Table 2**.

Figure 5. PHD2 P317R does not hydroxylate HIFαNODD, while PHD2 A228S has very minor enzymatic defects. An assay measuring hydroxylation of HIF1αODD (394-574) by PHD2 via NMR was performed. (A) Resonance shifting was monitored in real time to compare hydroxylation rates of A228S (blue), P317R (red) and WT (black) PHD2. PHD2 A228S displayed minorly impaired hydroxylation of both ODDs. PHD2 P317R displayed no activity on the P402 (NODD), while retaining near WT activity on P564 (CODD). (B) HSQC spectra display the resonance shifting pattern of HIF1a ODD upon prolyl hydroxylation catalyzed by PHD2 (WT, P317R, A228S) over the course of 20.2 h. Neighboring residues, A403 and I566, were used to monitor hydroxylation of P402 and P564 respectively. Spectra recorded at 0 h is shown in black while spectra recorded at the endpoint (20.2 h) is shown in red.

TABLES

Table 1. PHD2 mutant melting temperatures calculated via CD.

Table 2. MST determined dissociation constants between PHD2 mutants and HIFα CODD peptides.

Table 3. BLI determined binding constants between PHD2 WT and P317R and HIF1α NODD and CODD peptides.

Figure 1

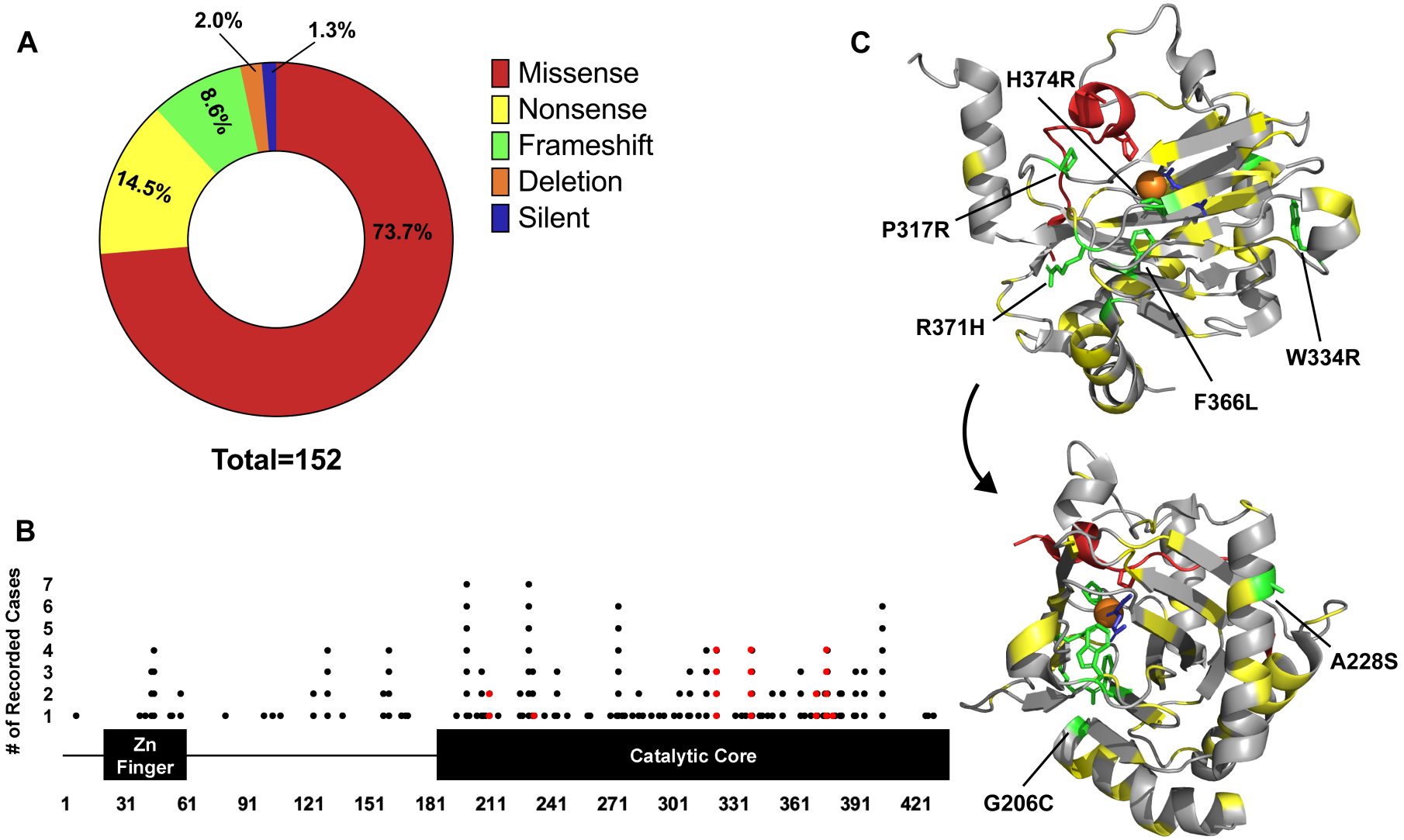
A
2.0%
1.3%
8.6%
14.5%
73.7%
Missense
Nonsense
Frameshift
Deletion
Silent
Total=152
B
# of Recorded Cases
7
6
5
4
3
2
1
Zn Finger
Catalytic Core
1
31
61
91
121
151
181
211
241
271
301
331
361
391
421
C
H374R
P317R
R371H
W334R
F366L
A228S
G206C

Figure 2

A

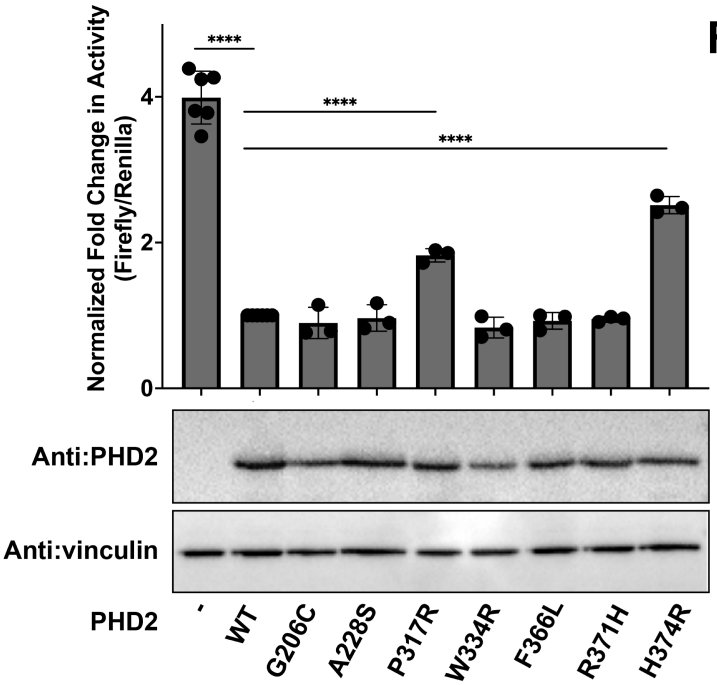
Normalized Fold Change in Activity (Firefly/Renilla)
****
****
****
0
2
4
Anti:PHD2
Anti:vinculin
PHD2
-
WT
G206C
A228S
P317R
W334R
F366L
R371H
H374R

B

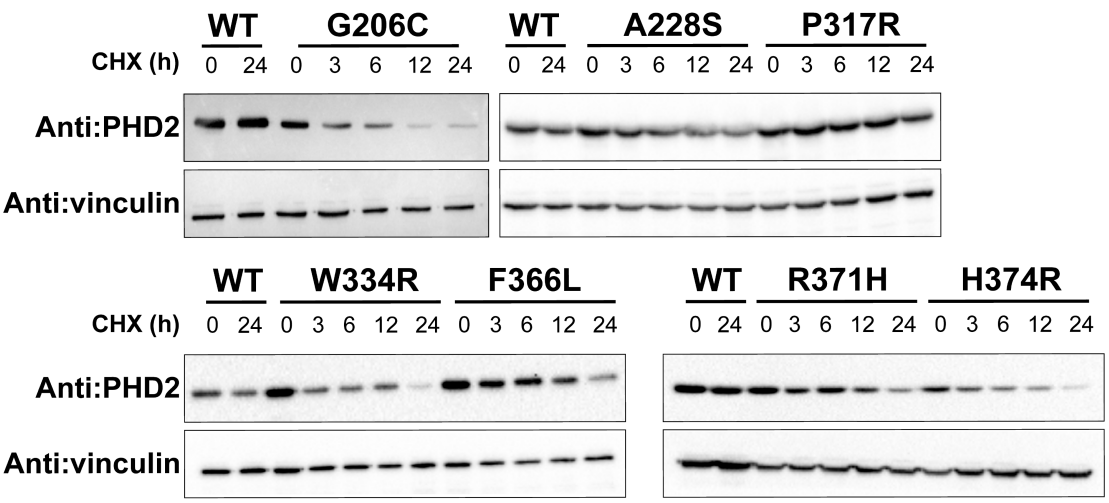
WT
G206C
WT
A228S
P317R
CHX (h)
0 24 0 3 6 12 24 0 24 0 3 6 12 24 0 3 6 12 24
Anti:PHD2
Anti:vinculin
WT
W334R
F366L
WT
R371H
H374R
CHX (h)
0 24 0 3 6 12 24 0 3 6 12 24 0 24 0 3 6 12 24 0 3 6 12 24
Anti:PHD2
Anti:vinculin

C

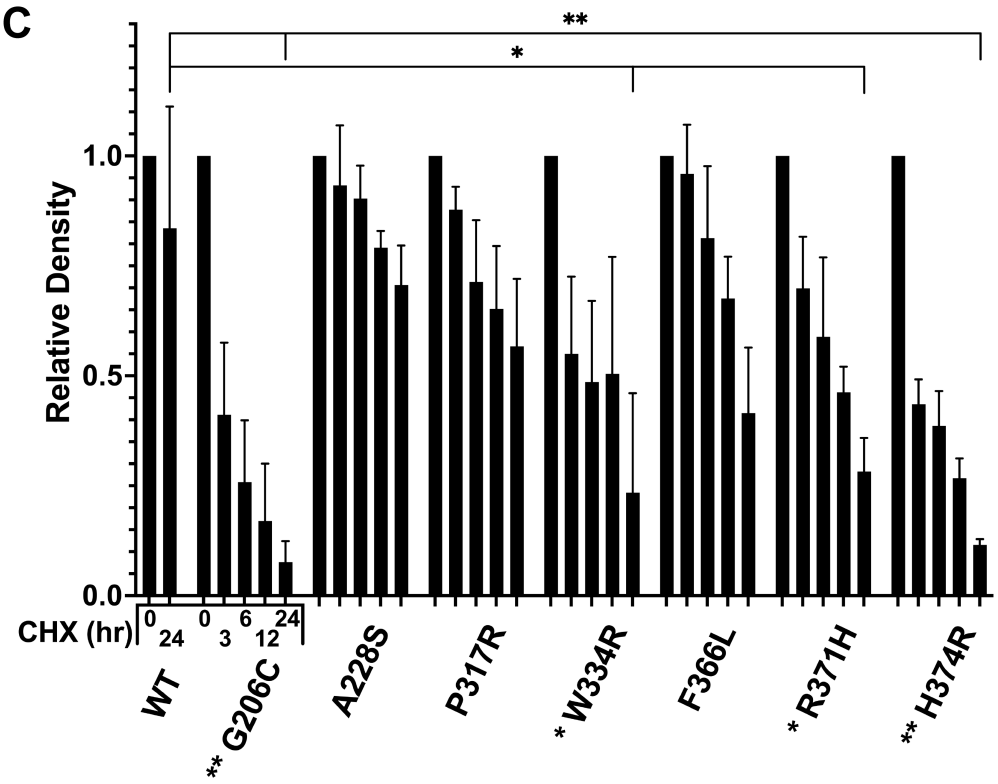
**
*
Relative Density
0.0
0.5
1.0
CHX (hr)
0 24 0 3 6 12 24
WT
** G206C
A228S
P317R
* W334R
F366L
* R371H
** H374R

Figure 3

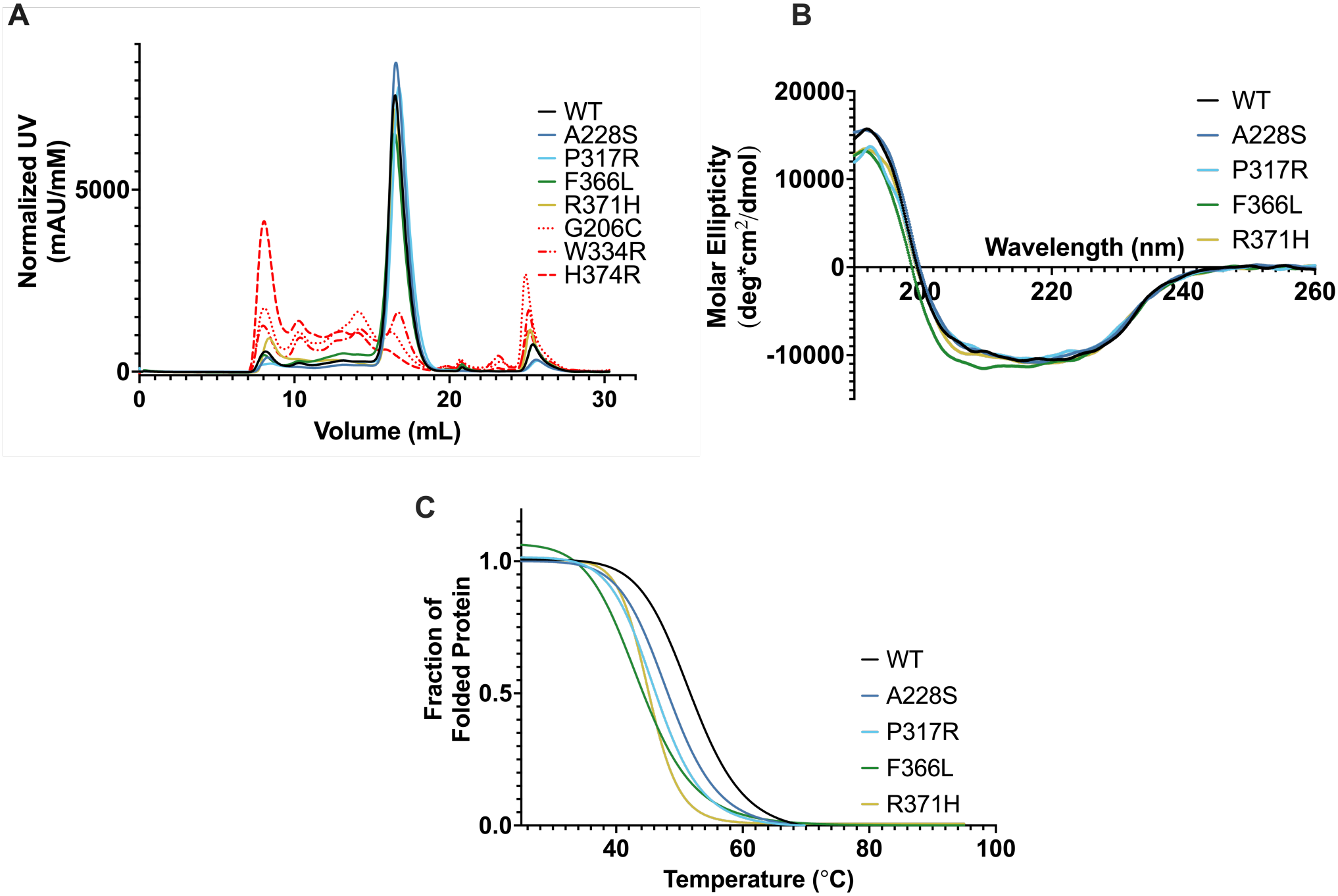
A
Normalized UV (mAU/mM)
5000
0
0
10
20
30
Volume (mL)
WT
A228S
P317R
F366L
R371H
G206C
W334R
H374R
B
Molar Ellipticity (deg*cm2/dmol)
20000
10000
0
-10000
Wavelength (nm)
200
220
240
260
WT
A228S
P317R
F366L
R371H
C
Fraction of Folded Protein
1.0
0.5
0.0
40
60
80
100
Temperature (°C)
WT
A228S
P317R
F366L
R371H

Figure 4

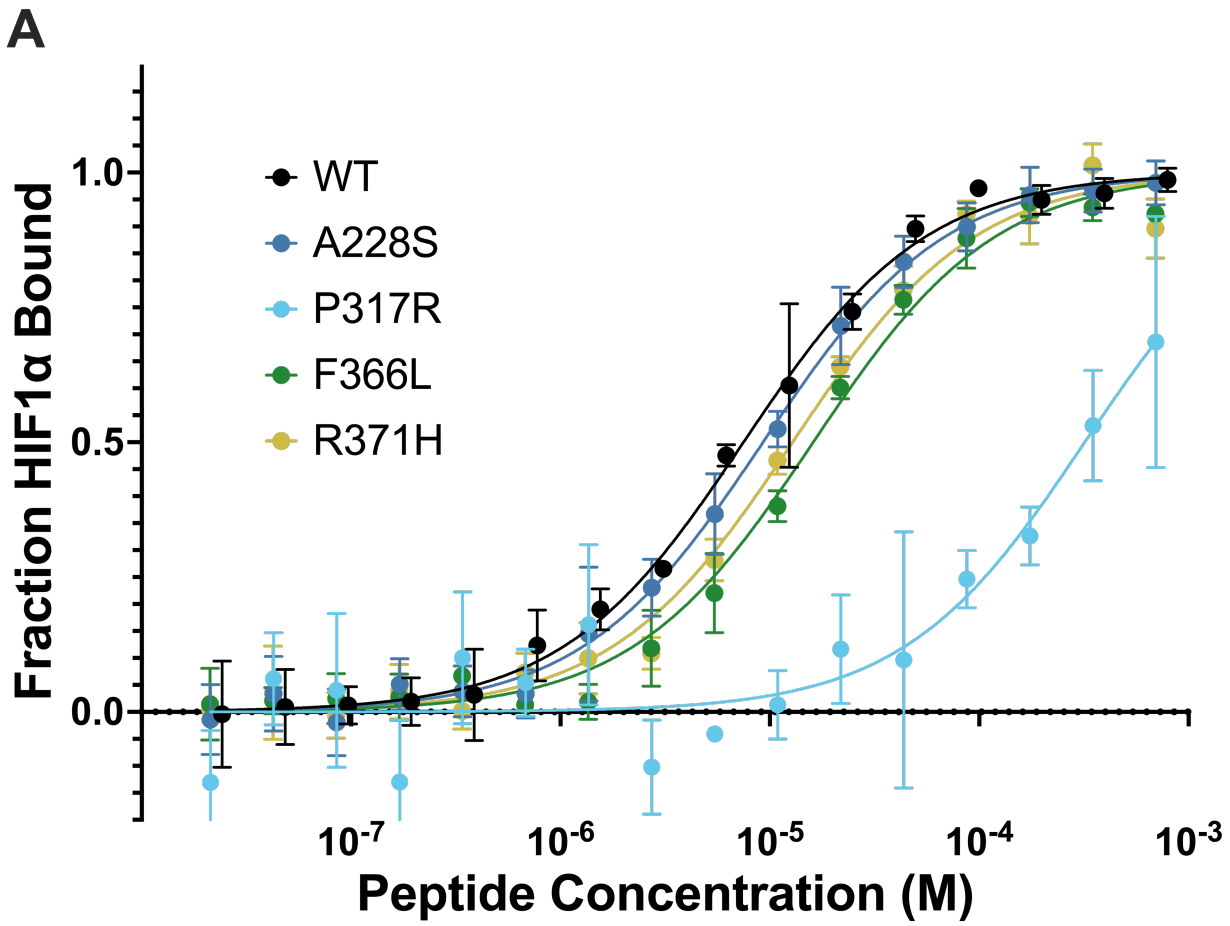
A
Fraction HIF1α Bound
1.0
0.5
0.0
WT
A228S
P317R
F366L
R371H
10-7
10-6
10-5
10-4
10-3
Peptide Concentration (M)

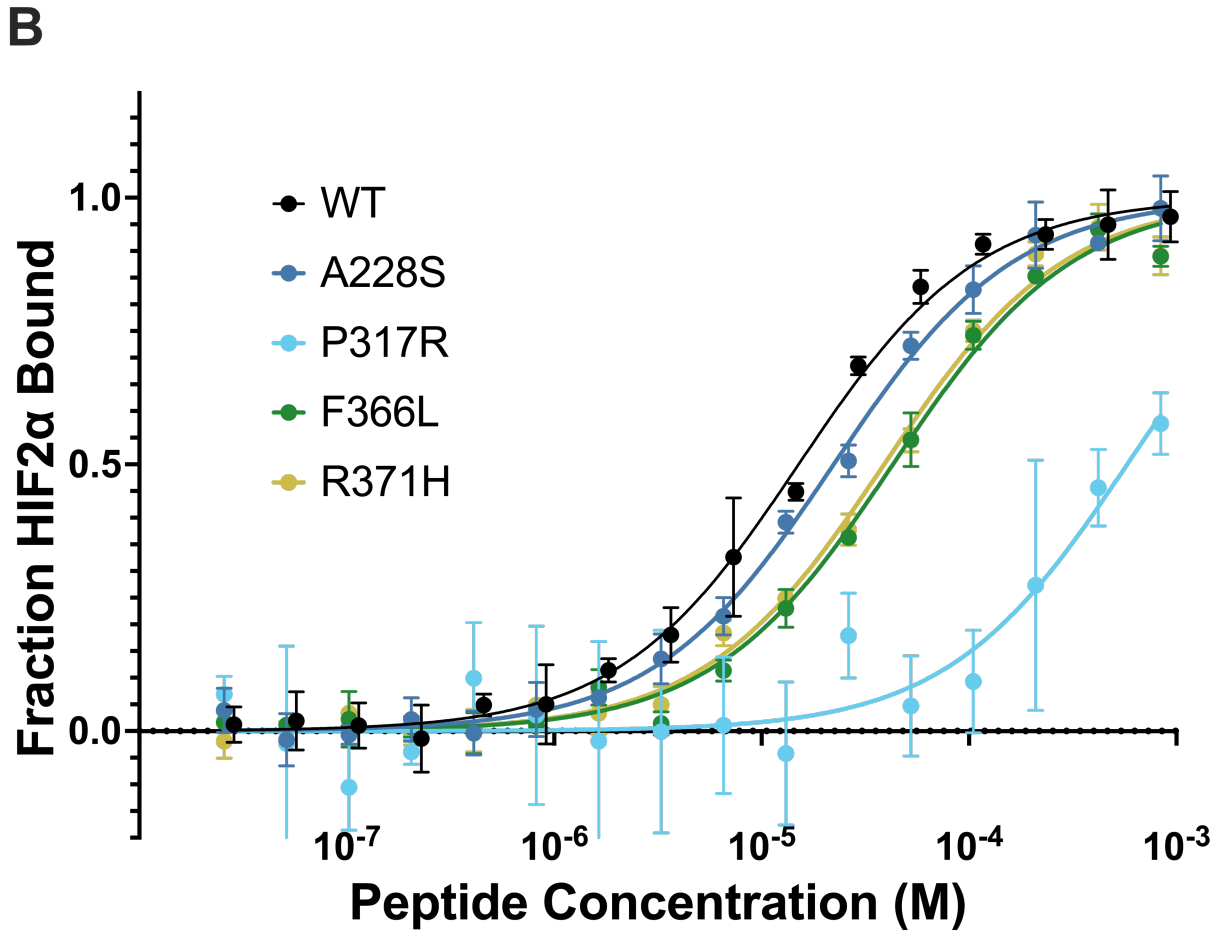
B
Fraction HIF2α Bound
1.0
0.5
0.0
WT
A228S
P317R
F366L
R371H
10-7
10-6
10-5
10-4
10-3
Peptide Concentration (M)

Figure 5

A

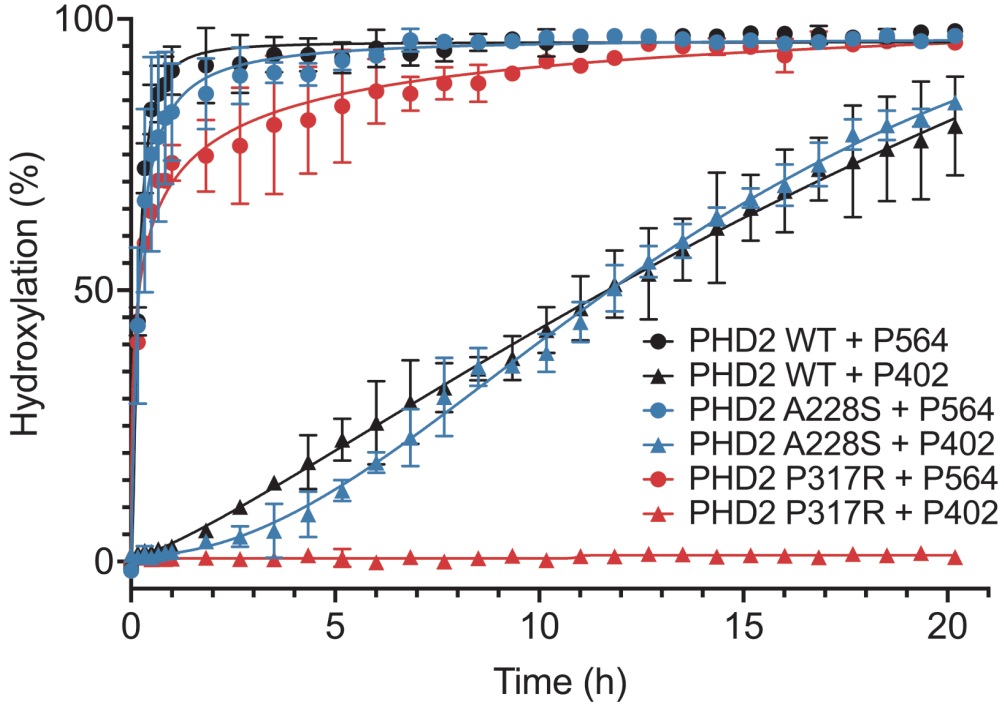
Hydroxylation (%)
100
50
0
0
5
10
15
20
Time (h)
PHD2 WT + P564
PHD2 WT + P402
PHD2 A228S + P564
PHD2 A228S + P402
PHD2 P317R + P564
PHD2 P317R + P402

B

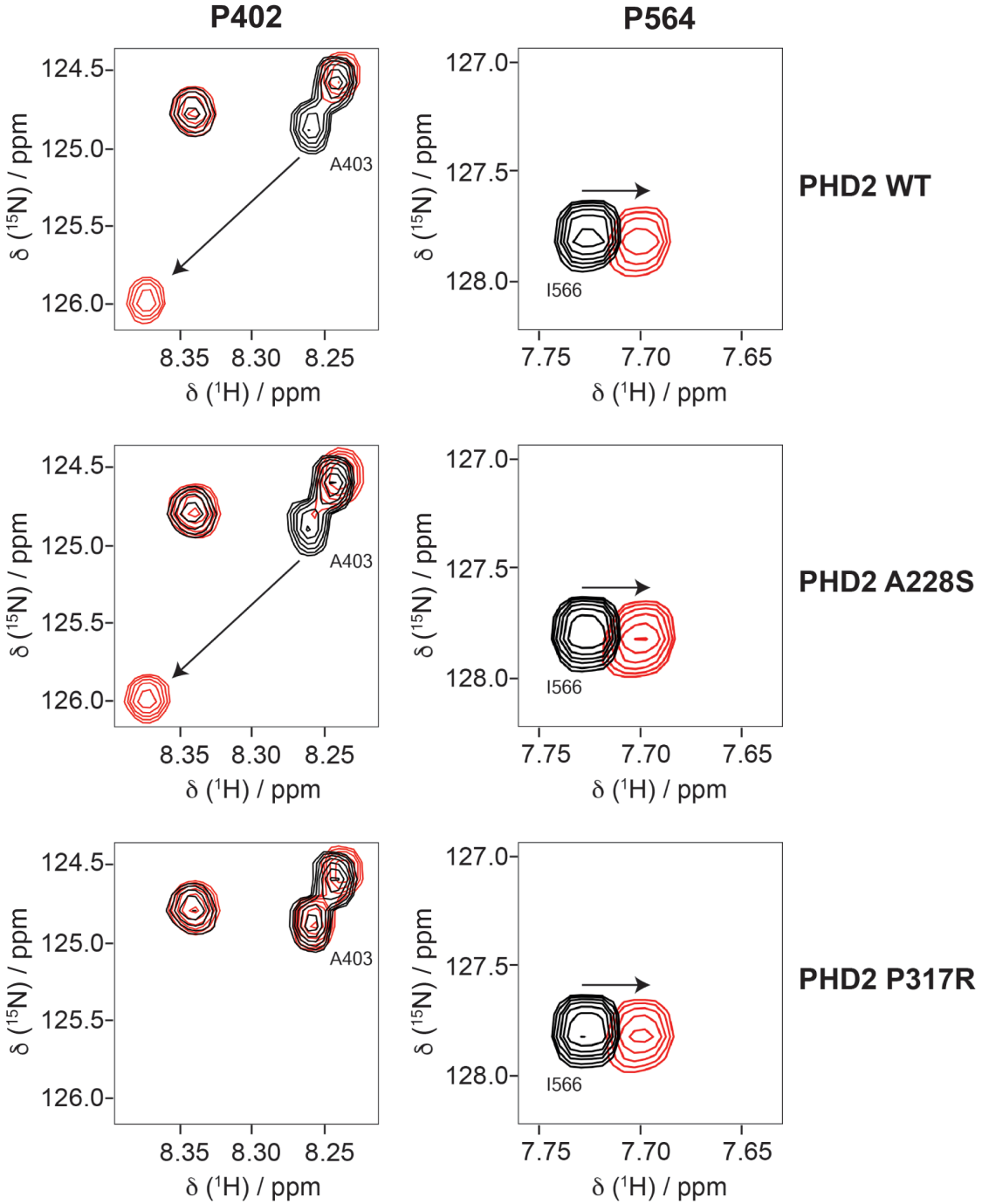
P402
P564
PHD2 WT
PHD2 A228S
PHD2 P317R
A403
I566
δ (15N) / ppm
δ (1H) / ppm
124.5
125.0
125.5
126.0
127.0
127.5
128.0
8.35
8.30
8.25
7.75
7.70
7.65

TABLES

Table 1. PHD2 mutant melting temperatures calculated via CD.

	T_m (°C)	R^2
WT	51.9	0.871
A228S	48.3	0.707
P317R	46.2	0.748
F366L	43.8	0.878
R371H	45.1	0.843

Table 2. MST determined dissociation constants between PHD2 mutants and HIFα CODD peptides.

	K_d (μM)	
PHD2	**HIF1α**	**HIF2α**
WT	7.5 ±0.52	15 ± 1.1
A228S	9.3 ± 0.57	22 ± 1.6
R371H	13 ± 1.6	39 ± 4.4
F366L	16 ± 1.8	43 ± 4.7
P317R	320 ± 20	580 ± 38

Table 3. BLI determined binding constants between PHD2 WT and P317R and HIF1α NODD and CODD peptides.

	K_d (μM)	k_a (x 10^4) (1/Ms)	k_d (x 10^{-3}) (1/s)
PHD2 WT + HIF1α CODD	2.1 ± 0.8	5.2 ± 1.4	101 ± 20
PHD2 P317R + HIF1α CODD	6.0 ± 0.7	0.21 ± 0.11	12.3 ± 5
PHD2 WT + HIF1α NODD	2.0 ± 0.8	0.26 ± 0.093	4.7 ± 0.2

PHD2 P317R + HIF1α NODD	2.0 ± 1.0	0.17 ± 0.049	3.0 ± 0.7

Supplementary Information

Peptide	Sequence
HIF1$\alpha_{555\text{-}574}$ CODD	DLDLEMLAPYIPMDDDFQL
HIF2$\alpha_{522\text{-}542}$ CODD	ELDLETLAPYIPMDGEDFQL
HIF1$\alpha_{395\text{-}411}$ NODD	DALTLLAPAAGDTIISLDF

Supplementary Table 1. Sequences of the HIF1α and HIF2α peptides used in the study. Peptides used for MST and BLI were N-terminally biotinylated.

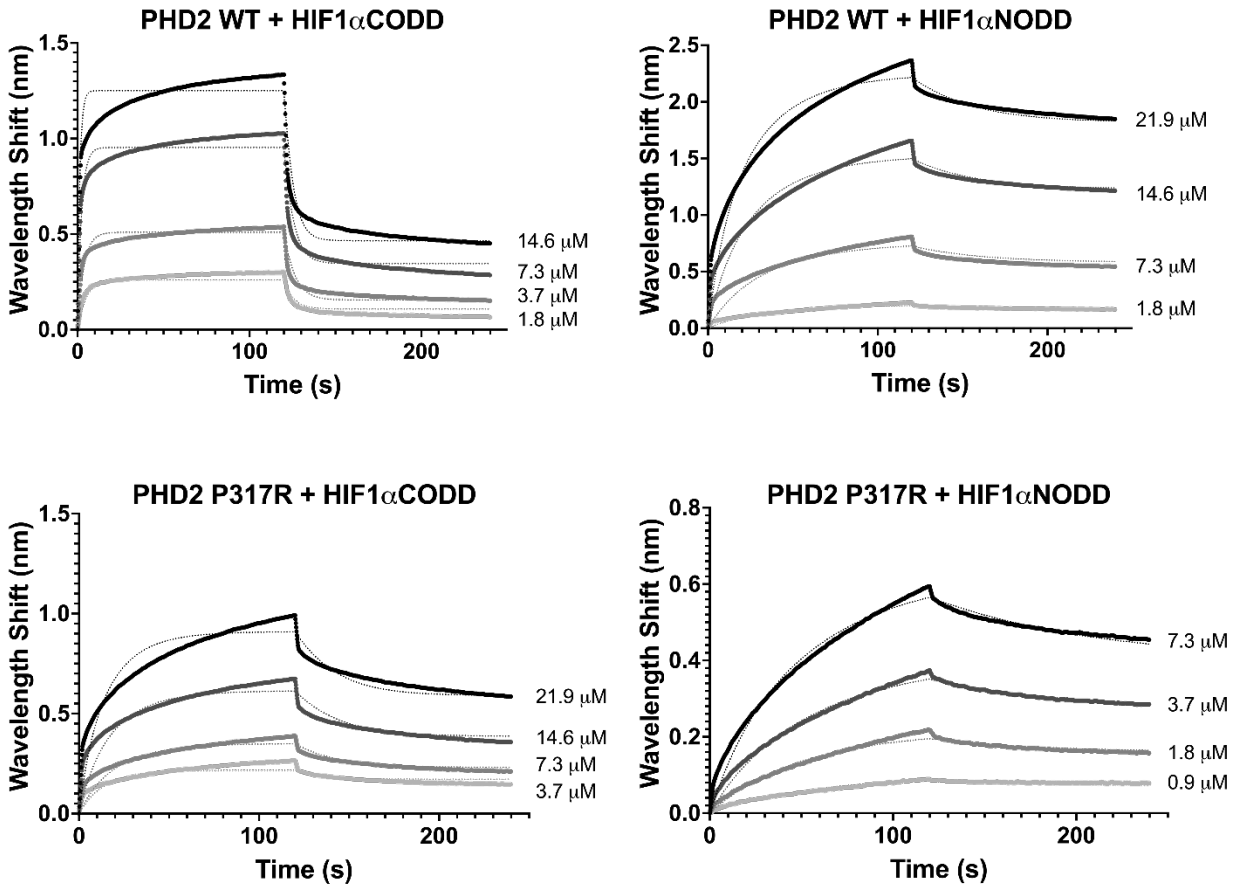

Supplementary Figure 1. Biolayer interferometry was performed to confirm the binding defect of PHD2 P317R observed via MST. Measurements with HIF1αCODD and HIF1αNODD peptides indicated that PHD2 P317R did not display a severe binding defect compared to PHD2 WT. While a minor defect was observed with HIF1αCODD and PHD2 P317R, no binding defect was observed with HIF1αNODD. Binding measurements were performed in technical triplicates.

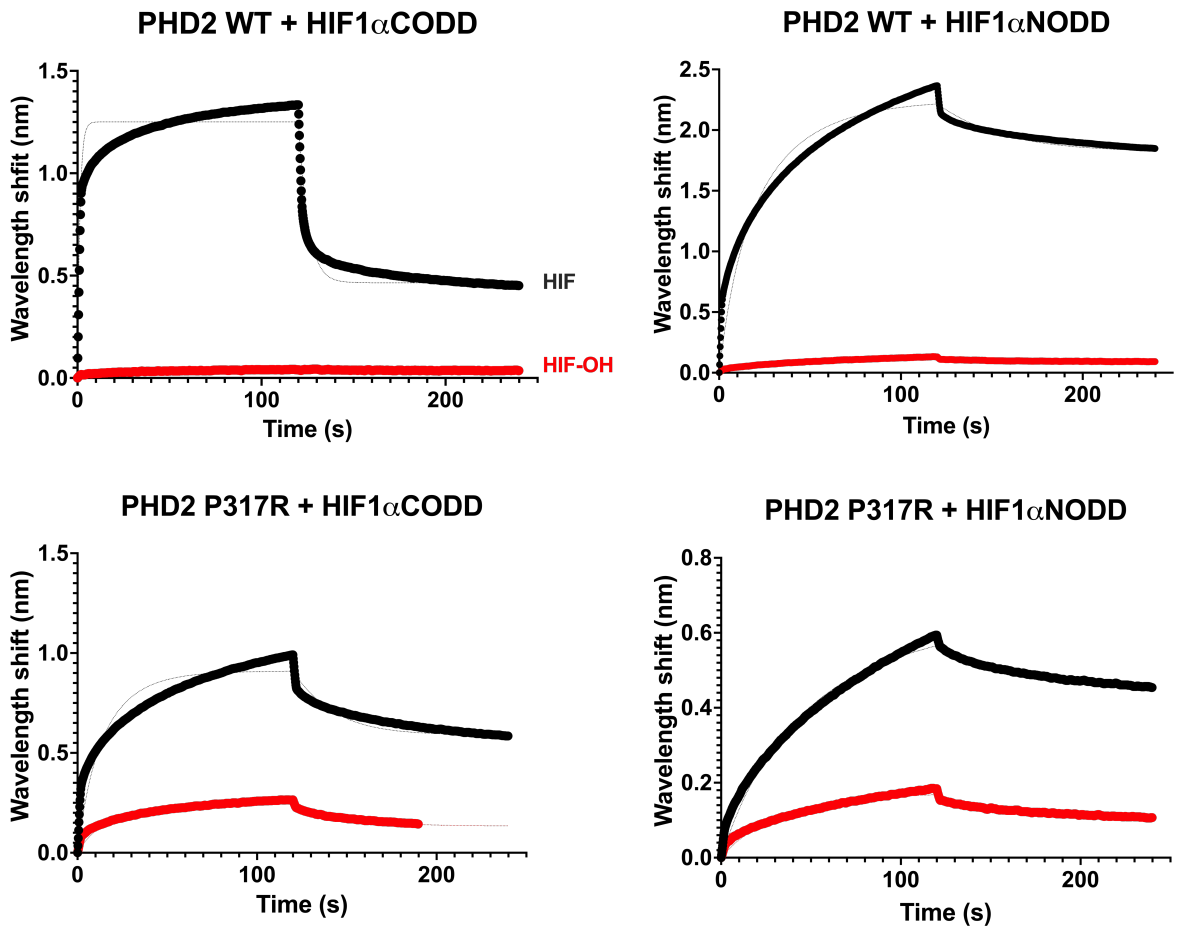

Supplementary Figure 2. Biolayer interferometry was performed with hydroxylated peptides as a negative control. As expected, no binding is observed with the hydroxylated peptides compared to unhydroxylated. Hydroxylated peptides are colored in red while unhydroxylated are black. The concentrations used for each experiment are as follows: PHD2 WT + HIF1αCODD: 14.6 μM, PHD2 WT + HIF1αNODD: 21.9 μM, PHD2 P317R + HIF1αCODD: 21.9 μM, PHD2 P317R + HIF1αNODD: 7.3 μM.

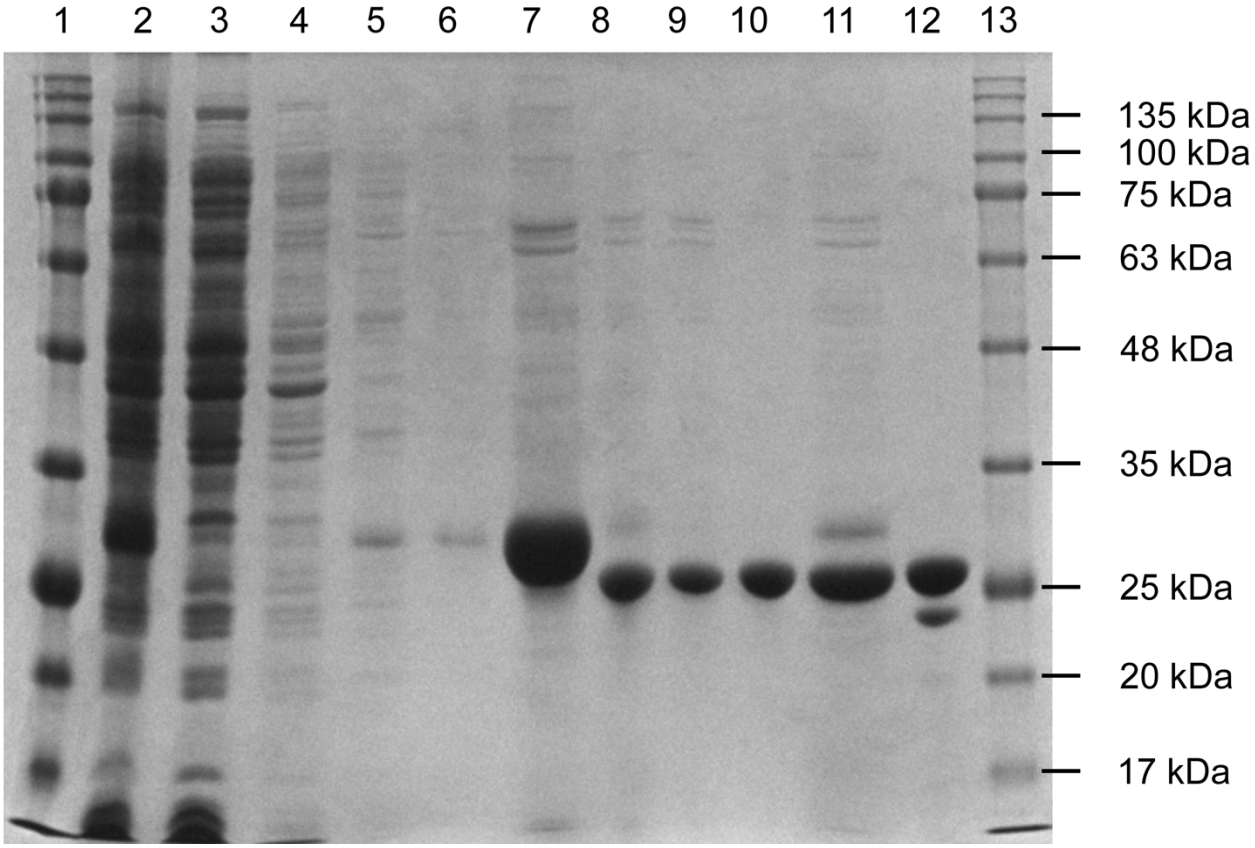

Supplementary Figure 3. Purification of PHD2 181-426. His_6-PHD2 (181-426) was expressed in BL21 (DE3) *E. coli* cells and purified using a Ni-NTA agarose and size exclusion column (SEC). 10 µl samples were taken throughout the purification and analyzed via Coomassie stained SDS-PAGE gel. The expected final size of His_6-PHD2 (181-426) is 27.76 kDa. (1) BLUelf prestained protein ladder, 15 µl (2) Lysate from BL21 (DE3) (3) Ni-NTA agarose flowthrough (4) Ni-NTA agarose 5mM imidazole wash (5) Ni-NTA agarose 30 mM imidazole wash 1 (6) Ni-NTA agarose 30 mM imidazole wash 2 (7) PHD2 elution from Ni-NTA agarose (8) Thrombin cleavage to remove His_6 tag (9) Reverse Ni-NTA agarose flowthrough (10) Reverse Ni-NTA agarose wash (11) Reverse Ni-NTA agarose elution (12) Pooled SEC fractions containing PHD2 (13) BLUelf prestained protein ladder, 5 µl.

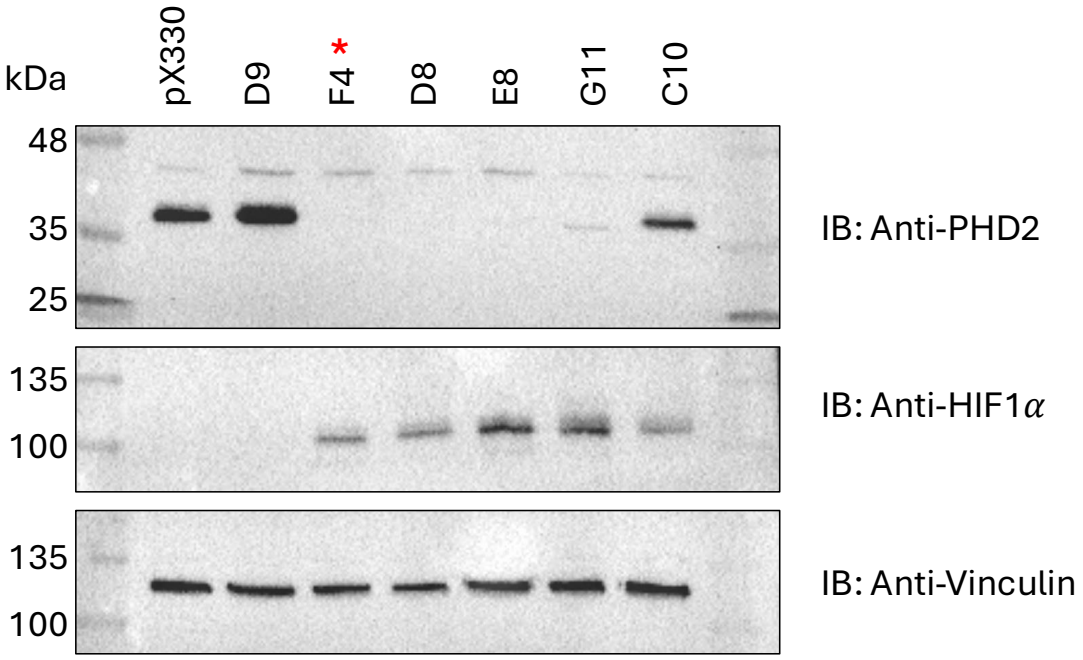

Supplementary Figure 4. Validation of PHD2 CRISPR KO in HEK293A cells. Homozygous PHD2 knockout (KO) HEK293A cells were generated via CRISPR. PHD2 KO was confirmed through immunoblotting. pX330 represents an empty plasmid without EGLN1 gRNA and is shown here as a positive control. Each lane represents single cell clones that were selected for PHD2 KO screening. HIF1α levels were also monitored. F4, D8, and E8 displayed complete loss of PHD2 along with HIF1α stabilization. F4, as indicated by asterisk, was chosen for use in further experiments.

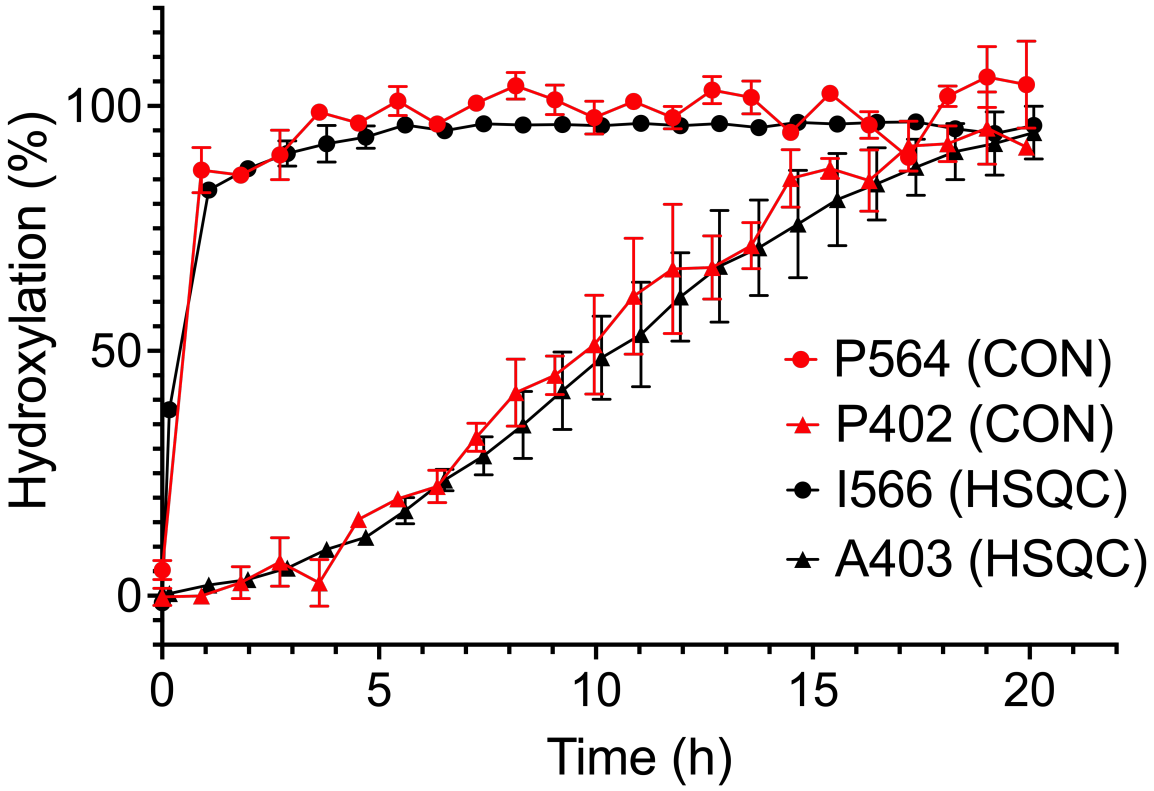

Supplementary Figure 5. Tracking proline hydroxylation using CON versus HSQC NMR. HSQC NMR was performed to monitor resonance shifting of ODD neighboring residues, I566 and A403, which were used as reporters for P564 and P402 hydroxylation, respectively. This method yields similar results as directly tracking proline hydroxylation using CON NMR, while requiring only HIF1α- ODD to be isotopically labelled. CON results are red, while HSQC results are black. Residues associated with CODD are represented with a circle and those associated with NODD are represented with a triangle.